EUROPEAN ORGANIZATION FOR NUCLEAR RESEARCH (CERN)

CERN-EP-2019-179
2019/09/30

CMS-PRF-18-001

Calibration of the CMS hadron calorimeters using proton-proton collision data at $\sqrt{s} = 13\,\text{TeV}$

The CMS Collaboration*

Abstract

Methods are presented for calibrating the hadron calorimeter system of the CMS detector at the LHC. The hadron calorimeters of the CMS experiment are sampling calorimeters of brass and scintillator, and are in the form of one central detector and two endcaps. These calorimeters cover pseudorapidities $|\eta| < 3$ and are positioned inside a solenoidal magnet. An outer calorimeter, outside the magnet coil, covers $|\eta| < 1.26$, and a steel and quartz-fiber Cherenkov forward calorimeter extends the coverage to $|\eta| < 5.2$. The initial calibration of the calorimeters was based on results from test beams, augmented with the use of radioactive sources and lasers. The calibration was improved substantially using proton-proton collision data collected at $\sqrt{s} = 7$, 8, and 13 TeV, as well as cosmic ray muon data collected during the periods when the LHC beams were not present. The present calibration is performed using the early 13 TeV data collected during 2016 corresponding to an integrated luminosity of 35.9 fb^{-1}. The intercalibration of channels exploits the approximate uniformity of energy deposit over the azimuthal angle. The absolute energy scale of the central and endcap calorimeters is set using isolated charged hadrons. The energy scale for the electromagnetic portion of the forward calorimeters is set using $\text{Z} \to \text{ee}$ data. The energy scale of the outer calorimeters has been determined with test beam data and is confirmed through data with high transverse momentum jets. In this paper, we present the details of the calibration methods and accuracy.

Submitted to the Journal of Instrumentation

*See Appendix A for the list of collaboration members

1 Introduction

Most precision studies of the standard model (SM) utilizing proton-proton (pp) collisions depend on reliable, precise measurements of jets and missing transverse momentum. The uncertainties in these are often related to the energy scale and the resolution of the measurement of hadron energy. For example, a precision measurement of the mass of the top quark requires a detailed understanding of the energy scale and resolution of jets; in a recent measurement of the top quark mass by CMS [1, 2], the single largest source of experimental uncertainty in two of the channels used was the jet energy scale. Another example is the measurement of the W boson mass, which requires a precise measurement of the underlying event [3]. Searches for physics beyond the SM (e.g., searches for dark matter based on measurements of jets produced through initial-state radiation [4]) often rely on measurements of hadron properties.

The methods used to calibrate hadron calorimeters have been studied and improved by several experiments. Previous publications from the CMS and ATLAS Collaborations on calorimeter calibration are reported in Refs. [5–10]. The hadron calorimeter (HCAL) [11, 12] is composed of four major subdetectors: the hadron barrel (HB) [13], the hadron endcap (HE) [11], the hadron forward (HF) [14], and the hadron outer (HO) calorimeters [8]. The CMS Collaboration has developed several techniques for calibrating its HCAL. The initial calibration makes use of results from several test beam exposures and from signals injected by dedicated calibration systems based on lasers and radioactive sources. Details of the test beam analyses and the calibration using radioactive sources can be found in Refs. [7, 9, 15]. The calibration of the detector is improved through the analysis of data from cosmic ray muons, taken when the CERN LHC was not operating, and data containing energy deposits from secondary particles produced during LHC beam tuning [16] and traversing the detector longitudinally.

The final calibration, described in this paper, uses information from collision data to further improve the precision of the calibration, and to establish a hadronic energy scale, which is stable over the course of the data taking. Because of the complex structure of the HCAL, its large angular coverage, nonuniformities in the amount of material in front of the calorimeters, and the limited acceptance of the CMS tracking system, these goals can only be achieved through the use of several techniques and data samples. In addition, the calibration needs to take into account nonlinearities in the HCAL energy response [9]. The calibration methods reported in this paper were first used with data collected during 2010–2015 at $\sqrt{s} = 7$, 8, and 13 TeV. Here, we report the calibration performed using data collected during 2016 at $\sqrt{s} = 13$ TeV, corresponding to an integrated luminosity up to 35.9 fb^{-1}.

Because of the nonlinear response of the HCAL, it is not possible to set an absolute energy scale that is valid for all incident hadron momenta. Although the response is closer to being linear at higher momenta, there are relatively few events available. Therefore, the calibration is performed with a sample of isolated hadrons of moderate momentum. The calibration of the HB and HE described in this paper yields a unit value for the relative energy scale factor of isolated charged pions with momenta of 50 GeV, which do not interact hadronically in the CMS electromagnetic calorimeter (ECAL). The energy of a reconstructed particle [17] is corrected for the calorimeter nonlinearity using a parametrization of the response as a function of transverse momentum (p_{T}), pseudorapidity (η), and the fractions of the particle energy deposited in the different subdetectors, as determined from a GEANT4-based [18] CMS detector simulation. Residual nonlinearities for jets are removed during the calibration of the jet energy scale [19]. The low-level calibration, reported in this paper, followed by the corrections and high-level calibration [17, 19], lead to the final jet energy calibration of the CMS calorimeter system.

Unlike the HB and HE, the HF does not suffer from a nonlinear energy response. The energy

scale for the HF is set to have a unit value of the relative energy scale factor for 100 GeV electrons and π^- mesons using test beam data [14].

The HO is used to measure the energy deposits from high-p_T particles whose showers are not fully contained in the ECAL and HB. The scale for the HO is set to give the best possible energy resolution for 300 GeV π^- mesons [8].

The calibration includes the following steps:

(i) the responses of different channels at the same η are equalized in the HB, HE, and HF, exploiting the approximate uniformity of energy deposits over the azimuthal angle (ϕ);

(ii) for the HB and the part of HE within the acceptance of the CMS tracking system ($|\eta| < 2.5$), isolated charged hadrons are used to equalize the η response and to set the absolute energy scale;

(iii) the η-dependent calibration for the electromagnetic portion of the HF is performed using electrons from decays of Z bosons; and

(iv) the responses of the HO channels are equalized across ϕ using muons from collision data, and the energy scale factor is validated using dijet events.

The paper is organized as follows. Section 2 provides a brief description of the HCAL. Section 3 describes the reconstruction of HCAL energies and of the physical objects used in the analysis. Section 4 gives information about the simulated event samples used in the design and testing of the calibration methods. The analysis of the symmetry in the azimuthal angle is in Section 5, and the calibration using isolated tracks is discussed in Section 6. The HF calorimeter calibration using $Z \to ee$ events appears in Section 7, and the intercalibration of the HO calorimeter and the validation of its energy scale factors are described in Section 8. A brief summary of the results is given in Section 9.

2 The CMS detector and its hadron calorimeter

The central feature of the CMS apparatus is a superconducting solenoid of 6 m internal diameter, providing a magnetic field of 3.8 T. Within the solenoid volume are a silicon pixel and strip tracker, a lead tungstate crystal ECAL, and the HB and HE calorimeters. Muons are detected in gas-ionization chambers embedded in the steel flux-return yoke outside the solenoid. In the barrel section of ECAL, an energy resolution of about 1% is achieved for unconverted or late-converting photons that have energies in the range of tens of GeV. For the remaining barrel photons the resolution is about 1.3% up to $|\eta| = 1$, deteriorating to about 2.5% at $|\eta| = 1.4$. In the endcaps, the resolution for unconverted or late-converting photons is about 2.5%, whereas the resolution for the remaining endcap photons is between 3 and 4% [20]. For isolated particles of $1 < p_T < 10$ GeV and $|\eta| < 1.4$, the track resolutions are typically 1.5% in p_T and 25–90 (45–150) μm in the transverse (longitudinal) impact parameter [21]. When measurements from the tracker and the calorimeters are used, the jet energy resolution amounts typically to 15% at 10 GeV, 8% at 100 GeV, and 4% at 1 TeV, to be compared to about 40, 12, and 5% obtained when only the ECAL and the HCAL calorimeters are used [17].

Events of interest are selected using a two-tiered trigger system [22]. The first level (L1), composed of custom hardware processors, uses information from the calorimeters and muon detectors to select events at a rate of around 100 kHz within a time interval of less than 4 μs. The second level, known as the high-level trigger (HLT), consists of an array of processors running a version of the full event reconstruction software optimized for fast processing, and reduces

the event rate to around 1 kHz before data storage.

A more detailed description of the CMS detector, together with a definition of the coordinate system used and the relevant kinematic variables, is reported in Ref. [12].

Figure 1 shows a schematic view of the layout of the CMS HCAL during the 2016 LHC operation at $\sqrt{s} = 13\,\text{TeV}$. The HB is located between radii of 1775 and 2876.5 mm and covers $|\eta| < 1.39$. The HB is divided into two half-barrels in the direction along the beam (z), each assembled from 18 wedges. Each wedge subtends 20° in ϕ and extends to 4330 mm from the CMS detector mid-plane. A wedge contains absorber plates made of brass (an alloy with 70% copper and 30% zinc) that are bolted together. The inner and outer plates are made out of stainless steel. There are 17 slots per wedge that house the plastic scintillator tiles. The inner and outer slots are 14 mm thick while the remaining ones are 9.5 mm thick. The HB has about 40 000 scintillator tiles. In order to limit the number of individual physical elements, the tiles at the same ϕ and depth are grouped into a single scintillator unit, referred to as a megatile. The megatiles in the first and last layers are of 9 mm thickness, while the remaining layers have 3.7 mm thick megatiles. Each megatile covers roughly 5° in ϕ. Of the four ϕ segments within a barrel wedge, the two segments at a larger radius are staggered with respect to the inner two. There is 61 mm of stainless steel between layers 0 and 1. There are 50.5 mm thick brass plates between adjacent layers 1–9, and the 56.5 mm thick brass plates up to layer 15. The back plate, which is in front of the last HB calorimeter layer, is made of 75 mm thick stainless steel. The megatiles are divided into 16 sections along the z axis, denoted by $|i\eta| = 1$ to 16, so that each tile corresponds to $\Delta\eta$ of 0.087. The set of scintillators corresponding to the same value of $i\eta$ and $i\phi$ (denoting the ϕ segment) in different layers are grouped together and referred to as a "tower". All 17 layers are grouped into a single readout channel until $|i\eta| = 14$, beyond which there are two depth sections, as shown in Fig. 1.

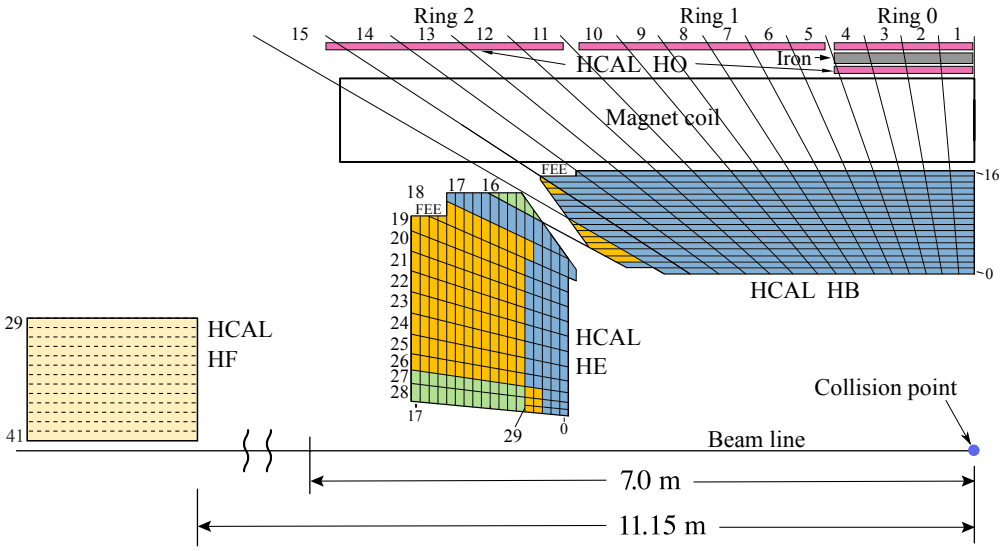

Figure 1: A schematic view of one quarter of the CMS HCAL during 2016 LHC operation, showing the positions of its four major components: the hadron barrel (HB), the hadron endcap (HE), the hadron outer (HO), and the hadron forward (HF) calorimeters. The layers marked in blue are grouped together as depth = 1, while the ones in yellow, green, and magenta are combined as depths 2, 3, and 4, respectively.

The HE calorimeter is also made of brass absorber plates with sampling layers of plastic scintillator. The innermost surface of HE is located 4006.5 mm from the interaction point and covers

$1.30 < |\eta| < 3.00$. Each endcap has an 18-fold symmetry in ϕ and has 34.5 mm thick sector plates each covering 20° in ϕ. The sector layers are separated by 9 mm thick brass spacers to allow space for the scintillator inserts. Each scintillator insert covers 10° in ϕ. The top edge of the front part of the endcap module has a slope of 53° corresponding to the gap angle between the HB and HE calorimeters. It also has a nose-like structure, with an additional layer of absorber and scintillator plate for $|i\eta|$ of 18, to increase the total interaction length for that tower. The absorber thickness between successive layers amounts to 78 mm of brass and scintillator, corresponding to the thickness of two sector plates and one spacer. The endcap on either side is divided into 14 parts along $|\eta|$, and the 18 layers are combined into 1, 2, or 3 depth sections, as shown in Fig. 1.

The HO calorimeter consists of one or two layers of scintillator outside the magnet coil. The entire assembly is divided into 5 rings, each having 12 sectors in ϕ. Six trays of scintillators are assembled on a honeycomb structure, which is then mounted in each of these sectors. The central ring (ring 0) has two layers of 10 mm thick scintillator on either side of a stainless steel block at radial distances of 3850 and 4097 mm, respectively. All other rings have a single layer at a radial distance of 4097 mm. The η-ϕ segmentation of the HO calorimeter matches closely that of the HB calorimeter. The HO calorimeter covers $|\eta| < 1.26$.

For the HB and HE calorimeters, clear fibers carry the light to hybrid photodiodes (HPDs) [23], and each HPD signal is digitized in 25 ns time intervals by a charge integrator and encoder (QIE) [24]. For the HO calorimeter, light is carried to silicon photomultipliers (SiPMs) and the SiPM signals are digitized by the QIEs.

The front faces of the HF calorimeters are located 11150 mm away from the interaction point on either side of the CMS detector and cover $2.9 < |\eta| < 5.2$. The detectors covering positive and negative η ranges are referred to as HF+ and HF−. The inner and outer radii of the HF calorimeter are 125 and 1570 mm, respectively. Each HF module is composed of 18 wedges made of steel with quartz fibers embedded along its length. The detection technique utilizes emission of Cherenkov light by secondary charged particles going through the quartz fibers. Long (1649 mm) and short (1426 mm) quartz fibers are placed alternately with a separation of 5 mm. The long fibers reach the front face of the calorimeter, while the short fibers start 12.5 radiation lengths into the calorimeter. These fibers are bundled at the back and led to a photodetector, and are grouped into 13 divisions in η on either side of the CMS detector and 36 divisions in ϕ, except the two largest $|\eta|$ sections, which contain 18 divisions in ϕ. While the HB and HE calorimeters work in conjunction with the ECAL for particle measurement, the difference in the energy deposits in the long and short fibers of the HF calorimeter functions as a separator between electromagnetic and hadronic showers. The light collected from an HF calorimeter fiber is converted to charge by a photomultiplier tube and digitized by the QIE.

3 Event reconstruction

In recorded events, signals from the HB, HE, and HO calorimeters are stored as 10 consecutive QIE measurements ("time samples", where each sample spans 25 ns). To reduce data volume and readout latency, a "zero suppression" mechanism is introduced that passes to the data acquisition system only those channels with at least one set of two consecutive samples above a threshold. The timing of the readout system is adjusted so that the triggered bunch crossing is in the fifth time sample. The data recorded from the HF channels are stored as four consecutive time samples, with the triggered bunch crossing in the third time sample. Energies are calculated as sums of time samples, after subtraction of the electronic pedestal and application of the calibration factor. For the HB and HE, and for the analysis described in Section 5.2, the

energy is calculated by applying a calibration factor to the sum of energies in the fifth and sixth time samples, with a containment factor to correct for the portion of the pulse extending beyond 50 ns. For the HF, since the Cherenkov pulse is shorter than 25 ns, only one time sample is used. For the HO, the energy is reconstructed as the sum of the fifth through eighth time samples. Because the HO pulse is longer than 100 ns, a containment correction is applied to account for signal beyond the eighth time sample.

The reconstruction also includes an algorithm that minimizes and corrects for contributions from additional interactions per bunch crossing, in the triggered as well as a few preceding or subsequent bunch crossings ("pileup"). Although the pulse shape for the HB and HE is the same as for HO, fewer time samples are used in HB and HE because there is a larger contribution from pileup for these detectors, and because the HPDs used for their readout have larger noise than the SiPMs. For the standard reconstruction of events used in physics analyses of CMS data, and for all the results in this paper, except for the one described in Section 5.2 (which uses the simple sum), a different method is used. In the presence of extra pileup interactions, the tails of the signals from interactions before the triggered bunch crossing can extend to the fifth time sample, contaminating the signal. To correct for this, the energy deposited in the triggered bunch crossing is obtained by fitting the time samples, after subtraction of the electronic pedestal, to up to three pulse shape templates. The reduction in the light output of the scintillator caused by radiation damage [25] and the decrease in the quantum efficiency of the HPD photocathodes caused by ion feedback damage [26] are monitored using a laser calibration system, and corrections are applied to the reconstructed hit energies based on the results of the monitoring.

There are several sources of noise in the hadron calorimeter, such as noise in the readout system, as well as noise from physical sources like particles other than optical photons interacting directly with the readout system. The electronic noise is measured and subtracted during the calibration procedure, whereas there are specific noise filters which handle all other types of noise. These filters eliminate either specific channels or entire events.

The reconstruction of physics objects produced in pp collisions starts with the reconstruction of particles. The CMS global event description is based on the particle-flow (PF) algorithm [17], which reconstructs and identifies each individual particle in an event with an optimized combination of information from the various elements of the CMS detector. In this process, the identification of the particle type (photon, electron, muon, charged or neutral hadron) plays an important role in the determination of the particle direction and energy. Photons, e.g., coming from π^0 decays or from electron bremsstrahlung, are identified as ECAL energy clusters not linked to any charged-particle trajectory extrapolated to the ECAL. Electrons, e.g., coming from photon conversions in the tracker material or from B hadron semileptonic decays, are identified as primary charged-particle tracks and potentially many ECAL energy clusters corresponding to this track extrapolation to the ECAL and to possible bremsstrahlung photons emitted along the path through the tracker material. Muons, e.g., from B hadron semileptonic decays, are identified as tracks in the central tracker consistent with either a track or several hits in the muon system that are associated with very low energy deposits in the calorimeters. Charged hadrons are identified as charged-particle tracks that are not identified as electrons or muons. The energy of a charged hadron is determined from the combination of the measurements from the tracker and the calorimeters. Finally, neutral hadrons are identified as HCAL energy clusters not linked to any charged-hadron trajectory, or as an excess in the combined ECAL and HCAL energy with respect to the expected charged-hadron energy deposit. The reconstructed particles are referred to as PF candidates.

For each event, hadronic jets (PF jets) are clustered from the PF candidates using the infrared and collinear safe anti-k_T algorithm [27, 28] with a distance parameter of 0.4. The jet momentum is determined as the vectorial sum of all particle momenta in the jet, and is found from simulation to be, on average, within 5 to 10% of its true momentum over the entire p_T spectrum and detector acceptance. The PF candidates associated with a jet are referred to as jet constituents. The PF missing transverse energy is calculated from the jet momenta as an imbalance of the energy flow in the transverse plane of the detector. Because PF makes optimal use of the detector information, contributions to the jet and missing transverse energy resolutions from charged hadrons are dominated by the precision of the momentum measurement from the tracker. The ECAL determines the contribution to the energy resolution from photons. However, for the highest energy charged hadrons, which can be produced in jets produced from decays of high mass new particles, for neutral hadrons, and for all particles at large rapidities, the hadron calorimeter dominates the momentum measurement. Accurate measurement of HCAL energies is also important in isolation calculations, which are used in particle identification.

During the 2016 data taking, the mean number of pp interactions per bunch crossing was approximately 23. The reconstructed vertex with the largest value of summed physics-object p_T^2 is the primary pp interaction vertex. The physics objects in this case are jets, clustered using the jet finding algorithm [27, 28] with the tracks assigned to the vertex as inputs, and the associated missing transverse momentum, taken as the negative vector p_T sum of those jets. Other reconstructed vertices are referred to as pileup vertices.

4 Simulated event samples

The methodologies used for the calibration are tested using simulated samples of pp interactions. Simulation of SM processes, unless otherwise stated, is performed with PYTHIA 8.206 [29] or MADGRAPH5_aMC@NLO 2.2.2 [30] event generators at leading order in the strong coupling, which is set to 0.130 at the Z boson mass scale. The event generators employ the NNPDF3.0 [31] parton distribution functions. Parton shower development and hadronization are simulated with PYTHIA using the underlying event tune CUETP8M1 [32]. Simulated samples consisting of single high-p_T particles are also produced. Samples that do not contain a collision in the nominal bunch crossing are used to simulate noise (see Section 5.2). The detector response is simulated using a detailed description of the CMS detector implemented with the GEANT4 package [18]. The simulated events are reconstructed with the same algorithms used for the data. The simulated samples include pileup with the distribution matching that observed in the data.

5 Calibration using azimuthal symmetry

The first step in the calibration of the HB, HE, and HF with collision data is to equalize the response in ϕ for each $i\eta$ ring and depth section. The procedure takes advantage of the approximate ϕ symmetry of the detector and the corresponding ϕ-symmetric energy deposit from minimum bias (MB) events (events selected with triggers designed to collect inelastic collisions with maximum efficiency while suppressing noncollision events). The layouts of the barrel and the endcap detectors have some ϕ dependence because of the absorber structure; the scintillator layers are staggered, and the absorber layers are also used as a part of the support structure. For the forward calorimeter, a radial shift in the beam spot position may also introduce asymmetry in the $i\eta$ rings close to the beam pipe, which can change with time. The relative contributions to the ϕ asymmetries from materials, inhomogeneous magnetic field, beam spot shift,

and miscalibration could, in principle, be understood using simulation. However, the material description in the simulation and the modeling of the beam spot position is not exact, and the difference between the actual detector and its Monte Carlo description can increase with time because of stresses from the magnetic field, gravity, etc..

Therefore the intercalibration is performed by comparing the average energy deposit in a calorimeter cell to the average energy deposit in the entire $i\eta$ ring. Two different calibration procedures are adopted.

Iterative method: A set of multiplicative correction factors (scale factors) for the uncalibrated energies are determined iteratively by equalizing the mean of the energies that satisfy both an upper and a lower threshold.

Method of moments: This intercalibration is carried out using MB events taken without zero suppression by comparing the first (mean) and second (variance) moments of the energy distribution in a calorimeter cell to the mean of the moments of the energy distributions in the entire $i\eta$ ring.

By construction, these two methods use events from disjoint data samples and are statistically independent.

The method of moments is performed using events with no zero suppression. The measured energies include contributions both from genuine energy deposits and from noise. The contributions due to noise are estimated from an independent data sample taken when there were no beam collisions (pedestal data), and subtracted from the measurements made using the collision data to extract the contribution due to signal. The iterative method, on the other hand, makes use of zero-suppressed events and is based on an estimation of mean energy in an energy interval. By definition the two methods symmetrize different energy ranges: low energy in the method of moments and high energy in the iterative method.

5.1 Iterative method

The data used in this method are selected from events triggered by subdetectors other than the HCAL to avoid trigger bias in the energy measurement; only events collected with electron, photon, and muon triggers are used. Results obtained from different triggers are compared, and the difference is used as input to the estimation of the systematic uncertainty.

This method utilizes energies recorded in HCAL channels that pass lower and upper threshold requirements. Figure 2 shows a typical energy spectrum obtained from reconstructed hit energy before the ϕ symmetry calibration. It is shown for a single channel in the HB (left) and the HF (right) calorimeters, along with the values of the lower and upper thresholds used for these subdetectors.

The reconstructed energies are obtained from zero-suppressed events after pedestal subtraction, and the corresponding mean noise level is zero. The value of the lower threshold (E_{low}) depends on the subdetector and is chosen to be well above the RMS of the noise distribution for a single channel, which is a few hundred MeV. The noise level is determined from pedestal data. For the HB and HE calorimeters, the threshold is 4 GeV, whereas it is 10 GeV for the HF calorimeter.

The upper threshold (E_{high}) ensures that statistical fluctuations in the tails of the energy distributions do not influence the mean. Its value also depends on the subdetector. For pp collision data, the threshold is 100 (150) GeV for the HB (HE and HF).

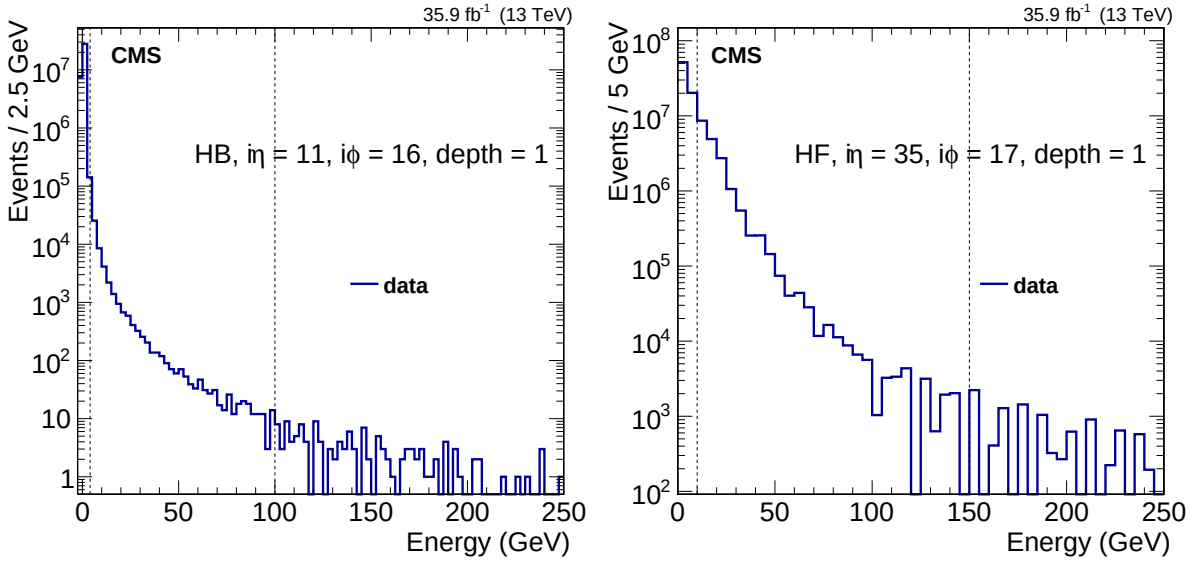

Figure 2: Energy spectra used as an input to the iterative method of equalizing the ϕ response of one typical $i\eta$ ring for an HB (left) and HF (right) calorimeter channel. Energy thresholds on the deposits used for the energy estimation are shown with dashed lines. The legends show the HCAL channel index in $i\eta$, $i\phi$, and depth segmentation units.

For each channel, the total energy between the thresholds E_{tot} is calculated from the observed energy spectrum using:

$$E_{\text{tot}} = \int_{E_{\text{low}}}^{E_{\text{high}}} \frac{\mathrm{d}N(E)}{\mathrm{d}E} E \mathrm{d}E, \tag{1}$$

and the mean cell energy ($\langle E_{\text{tot}} \rangle$) is defined as E_{tot} divided by the number of events used in the E_{tot} calculation. The scale factor is calculated as the inverse of the ratio of $\langle E_{\text{tot}} \rangle$ for that channel to the mean $\langle E_{\text{tot}} \rangle$ of all channels with the same $i\eta$ and depth, in each iteration. These scale factors are then applied to the energy measurement, and the whole process is repeated, including the selection of the cells included in the determination of E_{tot} through the application of the energy thresholds. This procedure is repeated until the mean change in the scale factor (over all channels) falls below a convergence cutoff value.

Figure 3 shows $\langle E_{\text{tot}} \rangle$ as a function of $i\phi$ for two typical $i\eta$ rings for the HB and HE calorimeters before and after the corrections. The spread in the mean cell energy $\langle E_{\text{tot}} \rangle$ is reduced from 4.7 to 0.3% for HB and from 6.2 to 0.2% for HE. The uncertainties in the scale factors are estimated from the statistical uncertainties in $\langle E_{\text{tot}} \rangle$ and the variation from the last iteration, added in quadrature.

The statistical uncertainties, including the variations from the last iteration, for the 2016 pp collision data are of the order of 1% for the HB, between 0.1 and 1.0% for the HE, and below 0.5% for the HF calorimeter channels, depending on $i\eta$ and depth.

5.2 Method of moments

The first two central moments of the energy distributions are used to obtain the scale factors for each channel. The main challenges in this method are (i) the noise exceeds the size of a typical signal, which is a few MeV in the HB channels and a few tens of MeV in the HE channels, and (ii) the variance of the noise distribution, 0.04–0.09 GeV ^{2}, differs considerably from one channel to another. Conditions are more favorable in the HF, where the noise variance is less

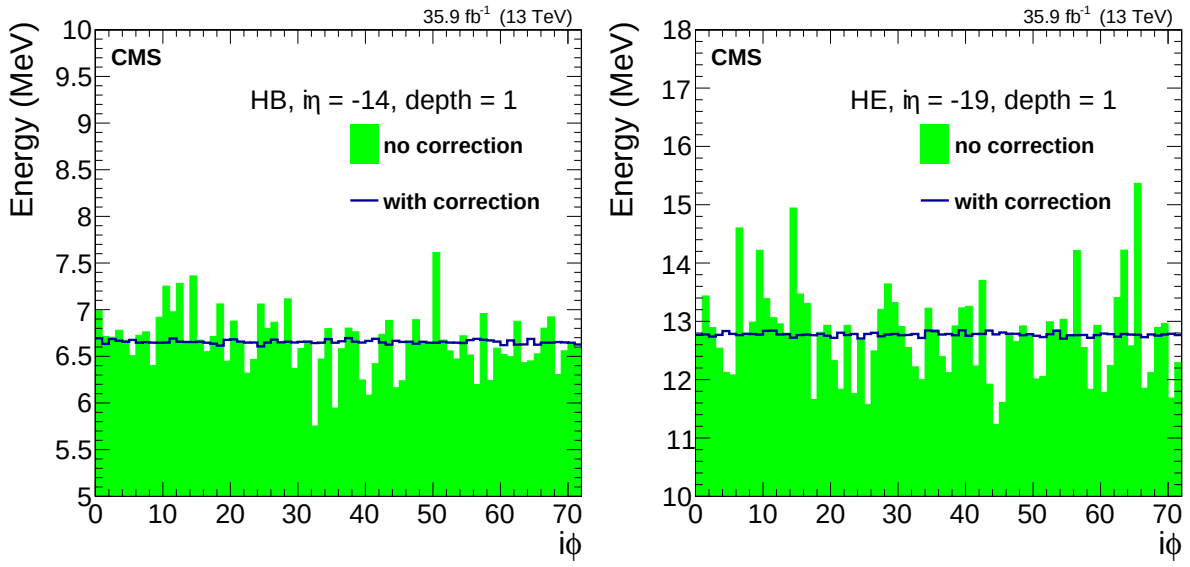

Figure 3: Mean cell energy $\langle E_{\text{tot}} \rangle$ for the iterative method measured before (solid histogram) and after (open histogram) correction as a function of $i\phi$ for a typical $i\eta$ ring of the HB ($i\eta = -14$, depth $= 1$, left) and of the HE ($i\eta = -19$, depth $= 1$, right) calorimeters. Data triggered using electrons, photons, and muon are used in this calibration procedure.

than the signal variance and also less than the mean value of the signal. Therefore, both the first and second moments for the HF calorimeter channels are used in the determination of the intercalibration constants.

The analysis is done using MB events taken with a special trigger where zero suppression is disabled in the HCAL readout. The noise in each channel is measured separately by using an independent data set taken when the LHC was not running and without any trigger requirements. The measured noise distribution is subtracted from the energy distribution after suitable normalization (pedestal subtraction).

The scale factor obtained using the first moment is given by

$$C_{i\eta,i\phi} = \frac{\langle E_{i\eta,i\phi} \rangle}{\frac{1}{N_\phi} \sum_{j\phi} \langle E_{i\eta,j\phi} \rangle}, \tag{2}$$

where N_ϕ is the number of HCAL towers in a given $i\eta$ ring, and

$$\langle E_{i\eta,i\phi} \rangle = \langle E^{\text{signal}}_{i\eta,i\phi} \rangle + \langle E^{\text{noise}}_{i\eta,i\phi} \rangle \tag{3}$$

is the mean energy deposited in the HCAL tower. After pedestal subtraction, the data are consistent with $\langle E^{\text{noise}}_{i\eta,i\phi} \rangle = 0$ and Eq. (3) becomes:

$$\langle E_{i\eta,i\phi} \rangle = \langle E^{\text{signal}}_{i\eta,i\phi} \rangle. \tag{4}$$

The uncertainty in the estimation of the first moment is given by

$$\sqrt{\Delta^2 \left(\langle E^{\text{signal}}_{i\eta,i\phi} \rangle \right) + \Delta^2 \left(\langle E^{\text{noise}}_{i\eta,i\phi} \rangle \right)}, \tag{5}$$

where Δ^2 is the variance. It is dominated by the uncertainty in the noise estimation. To achieve a precision better than 2% for channels in the middle of HB ($|i\eta| = 1$), a few tens of millions of events are required. While the method is straightforward to perform, a large amount of data is required to use it effectively. Figure 4 shows the scale factors obtained for a single HF tower using this method with data collected during 2016.

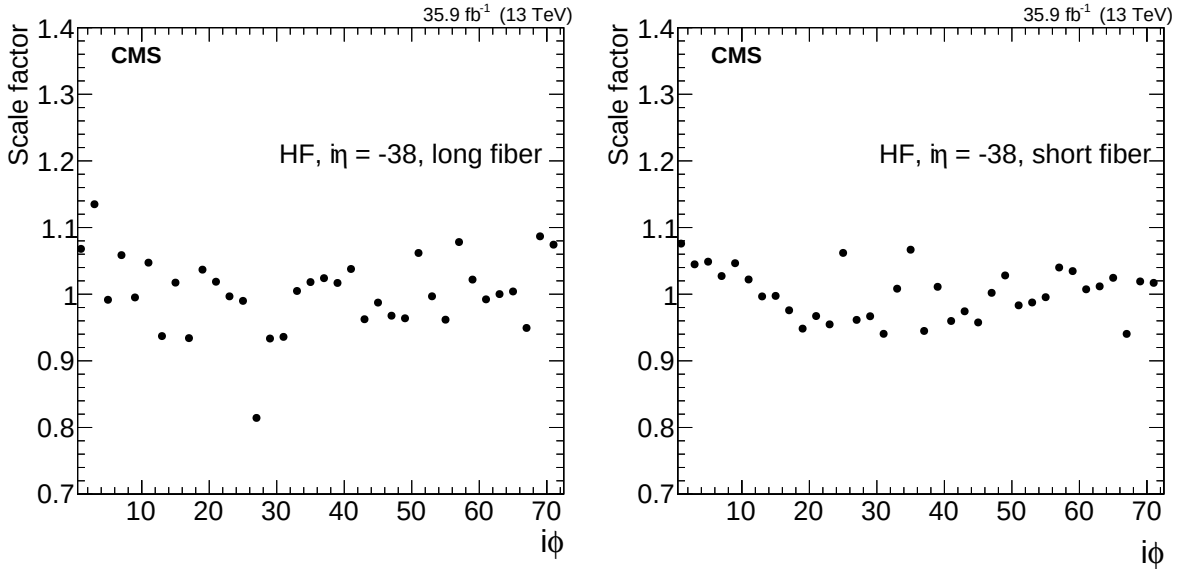

Figure 4: Calibration scale factor obtained using the method of moments with the first moment of the energy distribution for long (left) and short (right) fibers for two typical HF channels with $i\eta = -38$, as a function of $i\phi$. Only statistical uncertainties in the measurements are shown in these plots.

Estimation of the scale factor from the second central moment (variance) is done after removing the noise by subtracting the variance of the noise from the variance of the measured energy. The scale factor in this case is given by:

$$C_{i\eta,i\phi} = \sqrt{\frac{\frac{1}{N_\phi}\sum_{j\phi}\Delta^2 R_{i\eta,j\phi}}{\Delta^2 R_{i\eta,i\phi}}}, \tag{6}$$

where

$$\Delta^2 R_{i\eta,i\phi} = \langle \Delta^2(E^{\text{signal}}_{i\eta,i\phi}) + \Delta^2(E^{\text{noise}}_{i\eta,i\phi})\rangle - \langle \Delta^2(E^{\text{noise}}_{i\eta,i\phi})\rangle. \tag{7}$$

Assuming no correlation between the noise and signal depositions in the calorimeter,

$$\Delta^2 R_{i\eta,i\phi} = \langle \Delta^2(E^{\text{signal}}_{i\eta,i\phi})\rangle. \tag{8}$$

The minimum sample size for achieving a 2% uncertainty in the signal variance is determined by the residual noise contribution, and is of the order of a few million events. The method based on the second moment requires substantially smaller samples. Therefore, the second-moment method is used for the final results for HB and HE, but the results are still sensitive to the noise level in the channel, even when the noise levels are measured. During 2016, the noise levels for channels in the HF calorimeter were not measured, and the method based on the first moment is used for those channels.

Figure 5 shows the effect of using the first- or second-moment method on a simulated sample of MB events for the HB (left) and HF (right). The structure in the plot of HF scale factors as a

function of $i\phi$ reflects the geometry of the readout system (middle versus edge readouts) and of the passive material between the calorimeter and the interaction point (support structure and services for the detectors). The two methods of moments (mean and variance) have different sensitivities to the amount of material in front of the calorimeter. For HB and HE, the difference is typically $2.2 \pm 0.1\%$ on average, while for the HF calorimeter this difference is somewhat smaller, $0.8 \pm 0.1\%$ on average.

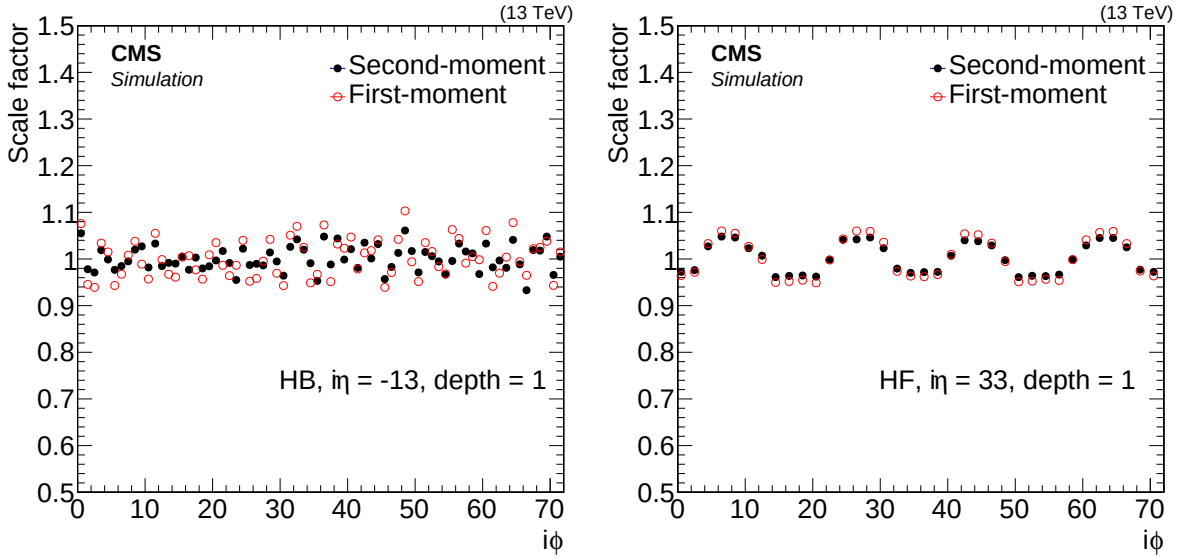

Figure 5: Derived calibration scale factors that equalize the ϕ response in a simulated sample of minimum bias events for a channel in the HB ($i\eta = -13$, depth $= 1$, left) and HF ($i\eta = 33$, depth $= 1$, right), as a function of $i\phi$ using two different methods: of first and of second moment.

Figure 6 shows the ratios of scale factors obtained in different portions of the 2016 data set from the second-moment method for two representative channels: $i\eta = 9$, depth $= 1$ in the HB, and $i\eta = 20$, depth $= 1$ in the HE. The plots indicate the level of stability of the scale factors over approximately six months of data taking.

5.3 Combination of the two methods

Figure 7 shows the ratio of the scale factors measured using the two methods (iterative method over method of moments) for the HB, HE, and HF calorimeters. The two sets of measurements agree within 5% as indicated from the RMS of the ratio distributions. The two sets of measurements agree, with the means of their ratios being 0.998 ± 0.001, 0.998 ± 0.001, and 1.004 ± 0.002 for the HB, HE, and HF calorimeters, respectively. The scale factor obtained from the method of moments has better precision for low-energy depositions, whereas those from the iterative method are better for high-energy depositions. The statistical uncertainties from the two methods are comparable for the HF calorimeter channels, whereas the iterative method gives smaller uncertainties for the HB and HE calorimeter channels. The uncertainty-weighted average of the scale factors from the two methods is used as the final scale factor for the HCAL ϕ intercalibration. The arithmetic mean of the corrections is used when the statistical uncertainties of both methods are below 1%. The weighted average (with weight $w = 1/\sigma^2$, where σ is the uncertainty in the measurement) is used otherwise. The systematic uncertainties in the inter-cell calibration performed with these combined results are estimated to be below 3%.

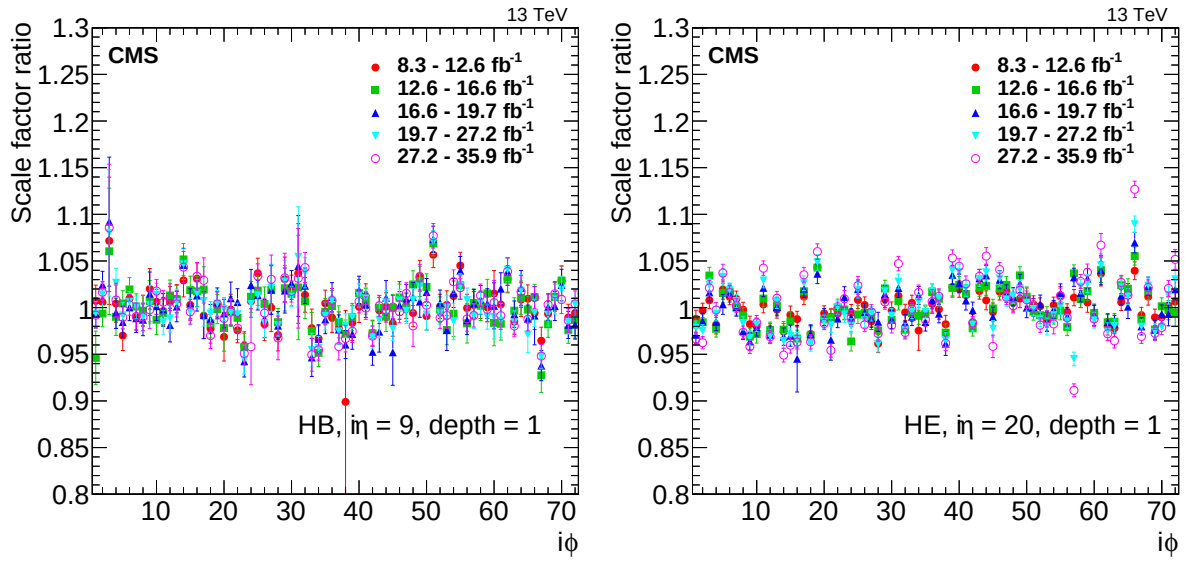

Figure 6: Ratio of the calibration scale factors for a typical HB ($i\eta = 9$, depth $= 1$, left) and HE ($i\eta = 20$, depth $= 1$, right) channels as a function of $i\phi$, in different data taking periods, to that obtained in a sample corresponding to the first 8.3 fb^{-1} of integrated luminosity accumulated during the run, for five data taking periods during 2016. Only statistical uncertainties in the scale factors are shown.

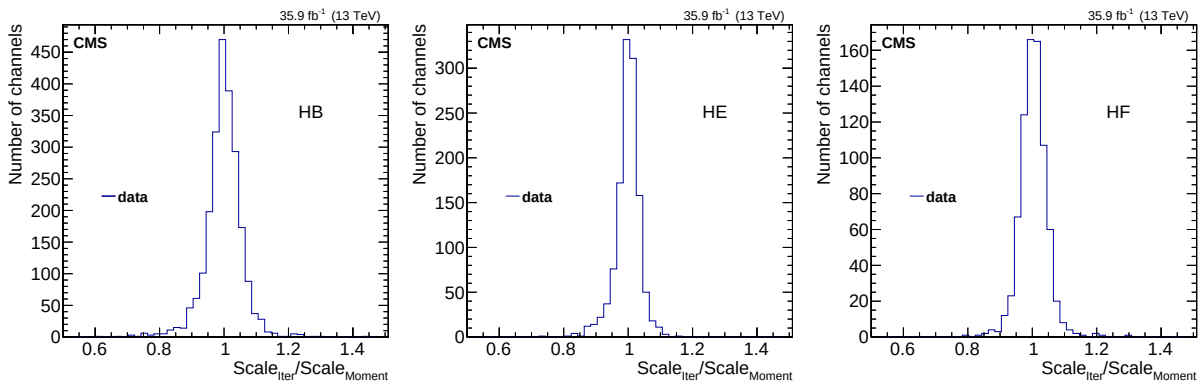

Figure 7: The ratio of ϕ intercalibration scale factors obtained with the method of moments to that obtained with the iterative method for HB (left), HE (center), and HF (right).

6 Absolute calibration using isolated tracks

The energies of charged hadrons in the central region of the CMS detector are measured by two independent detector systems: the trackers and the calorimeters. The precise calibration of the tracker system can be transferred to the calorimeter by comparing the two measurements. Unlike the momentum measurement by the tracker, the hadronic energy response of the HCAL is not linear. The nonlinearity is more pronounced at lower energies [9]. The goal of the HCAL absolute energy calibration is to set the relative energy scale to unity for 50 GeV charged hadrons that do not interact hadronically in the ECAL. In practice, the calibration is done with tracks of momentum between 40 and 60 GeV. The dominant systematic uncertainties are due to the contamination of the calorimeter energy from other hadrons, produced either in the same interaction that produced the isolated charged-hadron candidate or in pileup interactions.

The data used in this method come from two sources. The first sample is selected using a trigger designed for this analysis. At L1, the event is required to contain at least one jet with $p_{\mathrm{T}} > 60$ GeV. At the HLT, an isolated track with an associated energy in the ECAL below 2 GeV is required. The isolation calculation utilizes information from tracks after extrapolation to the calorimeter surface. The second sample uses events from the full, varied suite of CMS triggers. Events are selected offline using a filter that requires a track that satisfies very loose isolation criteria, has associated energy in the ECAL less than 2 GeV, and momentum higher than 20 GeV.

Events are required to have at least one well-reconstructed primary vertex [21] that is close to the nominal interaction point, with $r(\equiv \sqrt{x^2+y^2}) < 2$ cm and $|z| < 15$ cm. Tracks considered as candidate isolated hadrons are required to be associated with the primary vertex and to satisfy quality requirements. Their impact parameters are required to be close to the primary vertex in the transverse (xy) plane ($\Delta r < 200\,\mu$m) as well as along the beam axis ($\Delta z < 200\,\mu$m). The χ^2 of the track fit per degree of freedom is required to be less than 5, and the number of tracker layers used in the momentum measurement to be greater than 8. To confidently select tracks that have not interacted before reaching the calorimeter surface, tracks with missing hits in the inner and outer layers of the tracker are rejected.

The analysis uses isolation in a cone around the track to reduce contamination from neighboring hadrons, and to have a more accurate estimation of the hadron energy. The cone algorithm clusters energy based on the linear distance from the extrapolated track trajectory through the HCAL. For each HCAL tower, the distance between two points is determined. The first point is the intersection of the extrapolated track trajectory with the front face of the HCAL. The second point is the intersection of the tower axis (the straight line joining the center of the CMS and the center of the tower) with the plane perpendicular to the extrapolated track trajectory. If this distance is smaller than the radius of a circle on the surface of HCAL (R_{cone}), the energy from the HCAL tower is included in the cluster. The signal is measured using R_{cone} of 35 cm, which contains on average more than 99% of the energy deposited by a 50 GeV hadron.

The ECAL has a depth of approximately one interaction length and therefore more than half of the hadrons undergo inelastic interactions before reaching the HCAL. These hadrons are not used for calibration and are rejected by requiring the energy deposited within a cone of radius 14 cm around the impact point for the ECAL to be less than 1 GeV. This requirement also removes a large fraction of hadron candidates near a neutral particle, which deposit energy in the signal cone that would otherwise contaminate the measurement.

To further reduce contamination due to neighboring particles, an isolation requirement based on tracking information is used. The trajectories of all charged particles are propagated to the

ECAL surface. Hadron candidates are vetoed if there are additional tracks above a momentum threshold impacting the calorimeter surface within a circle of radius 64 cm around the candidate's impact point. The momentum threshold depends on the desired selection efficiency and purity. Two threshold values are used: a 10 GeV loose isolation requirement is used for the main analysis, whereas a 2 GeV tight isolation requirement is used in the assessment of systematic uncertainties. Although a stringent requirement on the isolation from neighboring charged particles would reduce the uncertainty caused by contamination of the signal energy from other nearby hadrons, the large number of pileup interactions at high instantaneous luminosity can result in a large amount of unrelated energy in the signal cone in the endcap region of the HCAL. The loose isolation requirement increases the efficiency for the track selection in the presence of pileup.

The calorimeter response is defined as the ratio

$$E_{\mathrm{HCAL}}/(p_{\mathrm{track}} - E_{\mathrm{ECAL}}), \tag{9}$$

where E_{HCAL} is the signal region energy of the HCAL cluster, E_{ECAL} is the energy deposited in the ECAL in a cone of radius 14 cm around the impact point of the track, and p_{track} is the momentum of the track. To mitigate the contamination from pileup, we apply a pileup correction, discussed below. The most probable value (MPV or mode) of the response is extracted using an iterative two-step fitting procedure to a Gaussian function. The two fits are performed in the intervals $\pm 1.5\sigma_{\mathrm{Tot}}$ and $\pm 1.5\sigma_{\mathrm{Fit}}$ around the mean of the distribution or the fitted mean, where σ_{Tot} is the sample RMS and σ_{Fit} is the width determined from the first fit.

The contribution from pileup is subtracted on an event-by-event basis by measuring the energy within an annular region beyond the signal cone. When there is a large amount of pileup energy near the cone, a relatively high pileup contribution is expected inside the cone. If so, the true particle energy is lower than that reconstructed in the cone. If the energy deposit outside the cone is caused by the particle itself, the true particle energy will be higher than the reconstructed energy in the cone. The track under consideration and the pileup originate from independent collisions within the same bunch crossing. From a study using simulated single isolated high-p_{T} pion events, the pileup contribution is related to the energy in a region around R_{cone} with an annular radius of $+10$ cm. It does not depend on the track momentum, and rather depends on the ratio of the energy in the cone to the track momentum. The corrected energy E_{cor} is calculated on an event-by-event basis using Eq. (10),

$$\begin{aligned} E_{\mathrm{cor}} &= E\left(1 + a_1 \frac{E}{p}\left(\frac{\Delta}{p} + a_2\left(\frac{\Delta}{p}\right)^2\right)\right), \\ (a_1, a_2) &= \begin{cases} (-0.35, -0.65) & \text{for } |i\eta| < 25, \\ (-0.35, -0.30) & \text{for } |i\eta| = 25, \\ (-0.45, -0.10) & \text{for } |i\eta| > 25, \end{cases} \end{aligned} \tag{10}$$

where E is the energy in the signal region cone $R_{\mathrm{cone}} = 35$ cm around the impact point of the selected isolated track, p is the track momentum, and Δ is the energy deposit in the annular region around the signal cone. The values for the constant depend on $|\eta|$ because of the tracker coverage and the $|\eta|$ dependence of the pileup particle energies. The values of the coefficients a_1 and a_2 are extracted using the dependence of the response on the ratio Δ/p by minimizing the difference between the mean corrected response for simulated samples that are processed two ways: with and without pileup. The pileup scale factors are derived using single pion simulated samples with and without pileup, and cross-checked with independent single pion simulated samples with pileup.

Figure 8 (left) shows the response distribution for the sample of simulated pions without pileup before and after application of residual energy scale corrections using the isolated track calibration technique. The bias in the mode of the energy distribution for the simulated pion sample that is caused by a pileup correction is less than 0.3%. The right plot in Fig. 8 shows the ratio of the modal value from a simulated single pion sample with pileup to that from a sample without pileup. The pions in the sample with pileup are required to satisfy the isolation criteria, and their analysis utilizes the pileup correction technique described above. The modes agree to within 1% for the entire calorimeter, and within 0.5% in the barrel region.

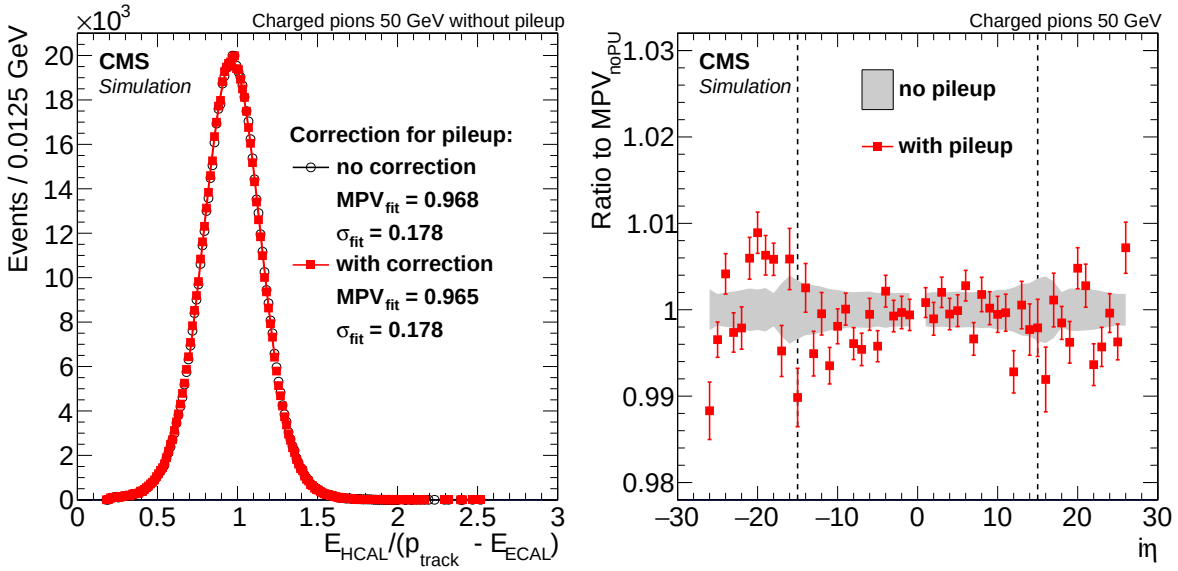

Figure 8: left: Distribution of the energy response in a simulated sample of single isolated high-p_{T} pions without pileup when the corrections for pileup have (red squares) or have not (black circles) been applied. The plot also shows the results of Gaussian fits. right: The ratio of the mode of the response distribution for a simulated pion sample with pileup, with loose charged-particle isolation, and the correction for pileup applied (red squares) to the mode from the sample without pileup. The uncertainties in the mode without pileup are shown with the gray band. Only statistical uncertainties are included. The dashed vertical lines show the boundaries between the barrel and the endcaps.

The calibration method utilizes an iterative approach. At the m-th iteration, the new scale factor $c_i^{(m+1)}$ is calculated using:

$$c_i^{(m+1)} = c_i^{(m)} \left(1 - \frac{\sum_j w_{ij}^{(m)} \left(\frac{E_j^{(m)}}{p_j - E_{j,\mathrm{ECAL}}} - \mathrm{RR} \right)}{\sum_j w_{ij}^{(m)}} \right), \tag{11}$$

where the sum is over events that contribute to the towers at the i-th $i\eta$ ring, RR is the reference to which the mean response is equalized, $E_{j,\mathrm{ECAL}}$ is the measured energy in the ECAL cluster around the track j, p_j is the track momentum, $w_{ij}^{(m)}$ is the weight of the particular tower with

measured energy e_{ij} in the cluster energy $E_j^{(m)}$:

$$w_{ij}^{(m)} = \frac{c_i^{(m)} e_{ij}}{E_j^{(m)}}, \qquad E_j^{(m)} = \sum_{i=1}^{n_j} c_i^{(m)} e_{ij}. \tag{12}$$

It follows from Eq. (11) that the iterative procedure results in equalization of the mean response of the detector around the value RR, which equals 1 by default. If the most probable value for the sample, $\text{mode}_{\text{sample}}$, differs from the sample mean, $\text{mean}_{\text{sample}}$, the reference response is set to $\text{RR} = \text{mean}_{\text{sample}}/\text{mode}_{\text{sample}}$. The formulation in Eq. (11) makes the procedure stable with respect to fluctuations of $E_j^{(m)}$.

The statistical uncertainty in the scale factor $\Delta c_i^{(m+1)}$ is estimated from the measured RMS of the response distribution $\Delta R_i^{(m)}$ for the subsample used for the i-th subdetector:

$$\Delta c_i^{(m+1)} = \Delta R_i^{(m)} \frac{\sqrt{\sum_j (w_{ij}^{(m)})^2}}{\sum_j w_{ij}^{(m)}}. \tag{13}$$

The procedure is iterated until the difference between the scale factors in subsequent steps becomes three times smaller than the statistical uncertainty.

The calibration procedure is applied to the 2016 collision data to obtain scale factors for each $i\eta$ ring through $i\eta = 23$. Scale factors for rings beyond $i\eta = 23$ in the HE are obtained by extrapolating these results. We note that the determination of the scale factors cannot be extended all the way to the boundaries of the tracker coverage, because the tracks used in the calibration are required to satisfy isolation criteria with respect to other particles, so the entire isolation cone is required to be within the tracker acceptance. Different criteria for selection of isolated hadrons and different methods for the pileup correction are tested, and the resulting correction factors for each data taking period are compared. The initial and resulting (after convergence) response distributions are shown in Fig. 9 for three HCAL η ranges. The resulting equalization of the mode is shown in Fig. 10. Equalization within $\pm 2.5\%$ is achieved with the iterative procedure for subdetectors up to $|i\eta| = 23$.

The statistical uncertainty in the scale factor, as obtained from data, is typically below 2%. The systematic uncertainty in the scale factor is estimated from the differences in the scale factors obtained (i) using tight and loose isolation criteria; (ii) using simulated isolated high-p_{T} pion samples with and without pileup; and (iii) using the true momentum versus the measured momentum of the charged particles in simulated events. The overall systematic uncertainty is around 2%.

7 Calibration of the HF using Z $\to$ ee events

The initial calibration of the HF was based on test beam data [14]. The energy scales of the long and short fibers in six HF wedges were set using the responses from 100 GeV electrons and negative pions. The scale was transferred to the rest of the wedges using radioactive source data.

The energy scale for the long fibers is validated using events from Z boson decays. The dileptonic decays of the Z boson are useful tools for checking the detector calibration, because the

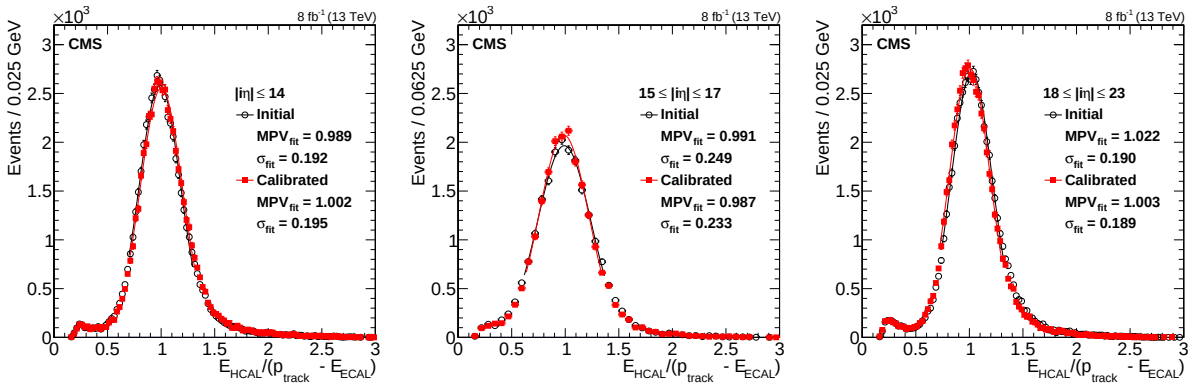

Figure 9: Response distributions for pions from 2016 data in three different η regions, $|\eta| \leq 1.22$ (left), $1.22 \leq |\eta| \leq 1.48$ (middle), and $1.48 \leq |\eta| \leq 2.04$ (right), with loose charged-particle isolation criterion: initial (black circles) and after convergence (red squares). Only statistical uncertainties are shown on the data points.

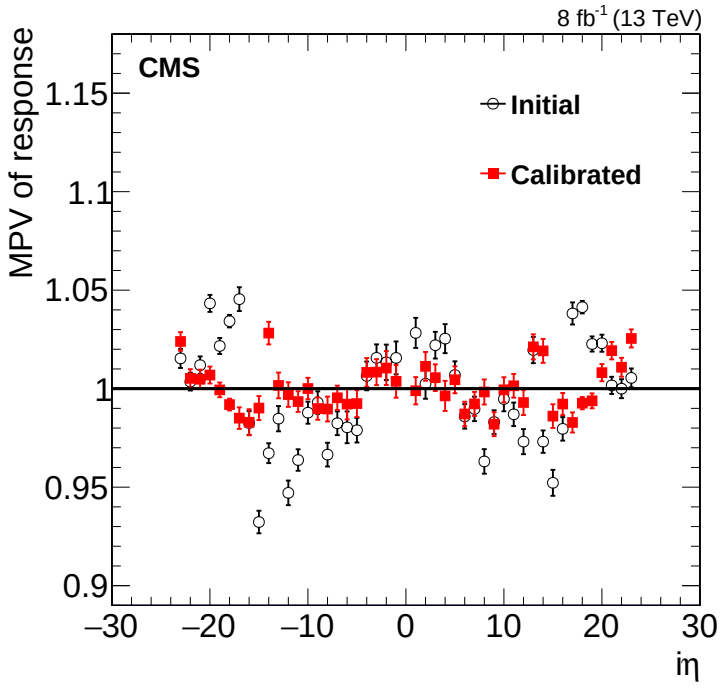

Figure 10: Modes of the response with their statistical uncertainties versus $i\eta$ from the 2016 data sample before (black circles) and after convergence (red squares). The loose charged-particle isolation constraint is applied.

production cross section of the Z bosons at the LHC is large, and the signature is almost background free. The dataset used for this calibration consists of events with one electron candidate in the HF and the other in the ECAL, which has been precisely calibrated. The scale of the HF long fibers is adjusted so that the dielectron invariant mass corresponding to the Z peak is consistent between simulation and data. The scale of the HF short fibers utilizes the short-to-long ratio measured in an analysis of 100 GeV test beam electron data.

Because the HF is outside of the tracker acceptance, the PF algorithm does not identify electrons that impinge on this detector and they are instead identified as photon candidates, which are clustered into PF jets. An isolated high-p_{T} electron, such as those produced in Z boson decays, would be identified as a jet by this algorithm. The reconstruction of HF electrons for this analysis, thus, starts with the PF jets. To select jets consistent with being isolated electrons, jets with characteristics consistent with those of anomalous energy deposits are rejected. Electron candidate jets must either have a nonzero hadronic or nonzero electromagnetic energy after zero-suppression is applied. The electromagnetic (EM) and hadronic (HAD) energies are defined by the deposits in the long (L) and short (S) fibers in the following way: EM = L$-$S, HAD = 2S.

Jets created from energy deposits of isolated electrons have a characteristic shower size $\Delta R \equiv \sqrt{(\Delta\eta)^2 + (\Delta\phi)^2}$ of about 0.15–0.2, where $\Delta\phi$ is in radians. Also, most of the energy is deposited in the long fibers, and the energy in the short fibers is small. Thus, HF electron candidates are required to have a "seed" for the core electron shower, chosen as the constituent of the PF jet with the largest energy. This seed defines the initial four-vector of the HF electron candidate. The four-vectors of other constituents of the PF jet, ordered in energy, are added to the four-vector of the HF electron candidate if the constituents are within $\Delta R = 0.15$ of the current four-vector of the core shower. The process stops when there are no more constituents close enough to the core shower. The choice of $\Delta R = 0.15$ to sample the core energy of the HF electron candidate is used to minimize the dependence on pileup. Because electrons from Z boson decays are expected to be more energetic than electron candidates arising from the misidentification of quark and gluon jets, the p_{T} of HF electron candidates are required to exceed 15 GeV. Furthermore, the electromagnetic fraction of the candidate's energy, calculated as a sum of all the EM energies of the PF constituents that form the core four-vector of the HF electron candidate, must be sufficiently large. The EM energy is required to be nonzero, and the ratio of the HAD to EM energy is restricted to be less than 1.20. The HF electron candidate is required to be isolated, as expected for leptons from Z boson decays. The total energy of all the PF candidates found in the vicinity of the shower, $0.15 < \Delta R < 0.30$, should not exceed 55% of the energy in the core shower. These requirements result in an efficiency of 62% for the selection of genuine electrons from Z boson decays, and retain only 1.5% of jets misidentified as electrons, as estimated using simulated Drell–Yan events.

Candidate Z boson events are selected by requiring only one isolated electron in the ECAL with $p_{\mathrm{T}} > 25$ GeV and with $|\eta| < 2.5$ [33]. The events are further required to have at least one HF electron candidate with $p_{\mathrm{T}} > 15$ GeV and $2.964 < |\eta| < 5.191$.

The dielectron invariant mass distributions ($M_{\mathrm{e^+e^-}}$) from candidate $\mathrm{Z} \to \mathrm{ee}$ events are shown in Fig. 11 for simulation and 2016 data. The Z boson mass is measured from a fit to a Gaussian function in a restricted mass region around the peak position. In both simulation and data, the measured Z boson mass is lower than the nominal mass (91.1876 GeV [34]) because only the long-fiber energies of towers within $\Delta R = 0.15$ of the seed are used, resulting in an underestimation of the shower energy due to energy leakage outside of this region. The HF energy scale in data is not adjusted to match the fitted mean from the invariant mass distribution using the

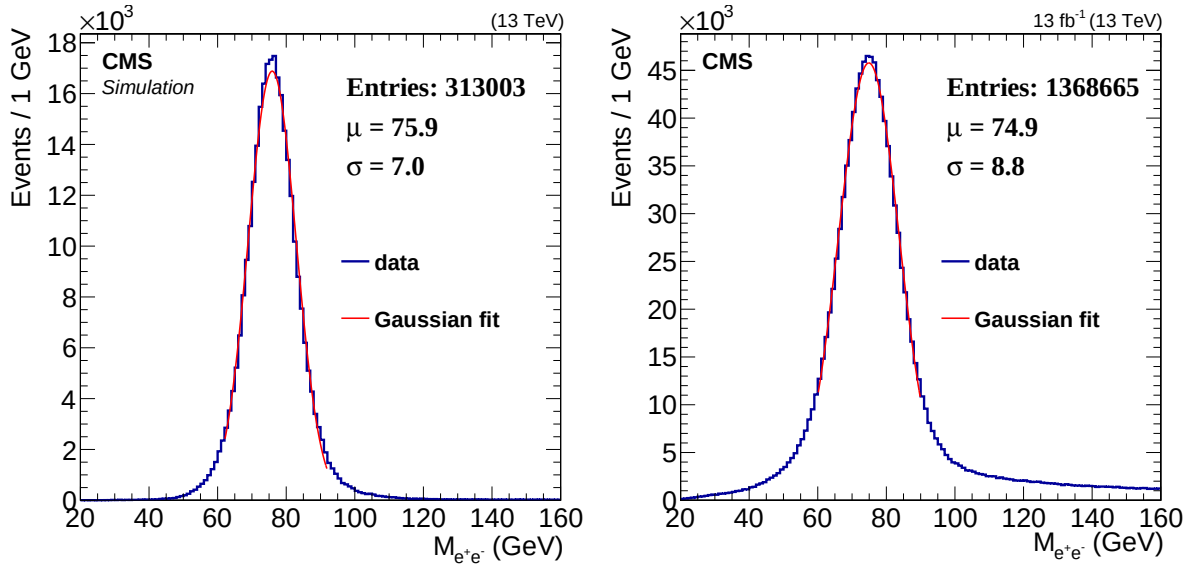

Figure 11: Invariant mass of the two electrons in candidate Z $\rightarrow$ ee events for simulation (left), and for 2016 data (right). One candidate is required to be in the ECAL, the other one in the HF. The mean (μ) and the width (σ) of the Gaussian fits are shown on the plots with their uncertainty. The quality of the fits is sufficient to extract the mean and the width to the necessary accuracies.

simulation, since both values are consistent within their uncertainties. Therefore no corrections are applied to the energy response in data. The 25% difference in the width between data and simulation is not yet fully understood, but selection of electron pairs in data from the Z boson decays, as well as shower mismodeling in the simulation, could cause this discrepancy.

The bias in the energy due to pileup is estimated using events with different numbers of pileup interactions. The result is consistent with a shift of the measured Z boson mass of up to 1%.

Figure 12 shows the dielectron invariant mass as a function of the HF electron candidate $|i\eta|$, for $i\eta$ values between 30 and 38. The HF energy response in data for both HF+ and HF$-$ are similar. The energy response in the simulation has a shape similar to that of the data, but there is a visible trend: for the towers with $|i\eta| = 33$–38, the data show a lower energy scale than the simulation. This deviation is not completely understood and therefore no specific corrections are considered at the moment.

8 Calibration of the HO calorimeter

The calibration of the HO calorimeter is carried out in two steps. The intercalibration makes use of muons from collision data, as well as cosmic ray muons that traverse the tiles of the HO. The determination of the absolute energy scale makes use of dijet events.

8.1 Intercalibration of the HO towers

Before data taking began, the intercalibration of the HO towers was performed by equalizing signals from cosmic ray muons. This method has a few drawbacks:

- large statistical uncertainties in the calibration of the HO towers near $i\phi = 1$ and 37 because there are few horizontal muons in the cosmic muon sample;

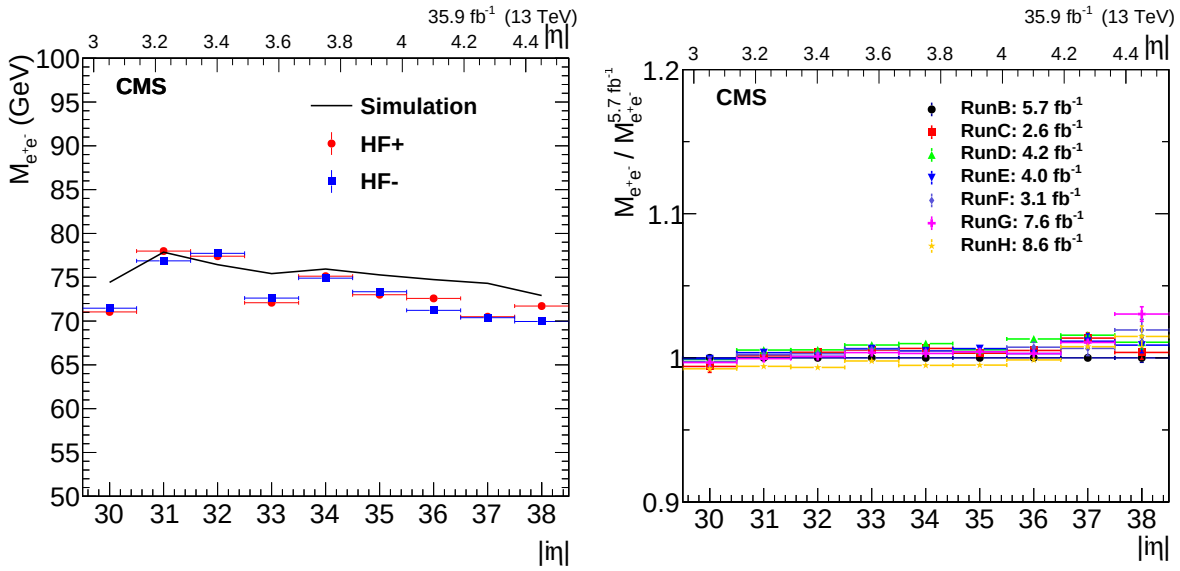

Figure 12: (left) The results of the fits of the dielectron invariant mass to a Gaussian function for different η values of the HF electron candidates obtained in simulation (black line, combined HF+ and HF−) and 2016 data, split by HF+ and HF− (red and blue, respectively). (right) The results of the fits of the dielectron invariant mass to a Gaussian function for different pseudorapidity η values of the HF electron candidates obtained in data corresponding to different run ranges. The dielectron mass in the denominator comes from the first run range corresponding to 5.7 fb^{-1}. Errors on the data points are statistical only.

- a large uncertainty in the extrapolated track position in the HO, which was based on standalone muon reconstruction using information from muon chambers alone; this leads to a large uncertainty in the resulting calibration.

The intercalibration is improved using muons from W and Z decays in pp collisions. Muon candidates [35] are selected using the following criteria:

- the associated track is well measured and satisfies reconstruction quality criteria;
- the energy in the calorimeter tower traversed by the muon is consistent with the expectation of a minimum ionizing particle;
- the muon is isolated: no other reconstructed muon is present within a 15° cone around the muon under study and the scalar p_{T} sum of all other tracks within $\Delta R < 0.3$ relative to the muon is less than 4 GeV;
- the momentum of the muon after extrapolation to the HO face is more than 15, 17, and 20 GeV for towers in rings 0, ±1, and ±2, respectively;
- the cosine of the angle made by the muon trajectory with respect to the HO scintillator surface is more than 0.6 (0.4) for ring 0 (other rings);
- the location of the muon after extrapolation to the HO is at least 2 cm away from the tower boundary; and
- the time of the HO energy deposits is within 30 (20) ns of the beam crossing time for towers in ring 0 (other rings).

Figure 13 shows a typical distribution of the energy deposited in a tower impacted by a muon, for two typical HO towers. The signal distribution is parametrized in the pedestal region with

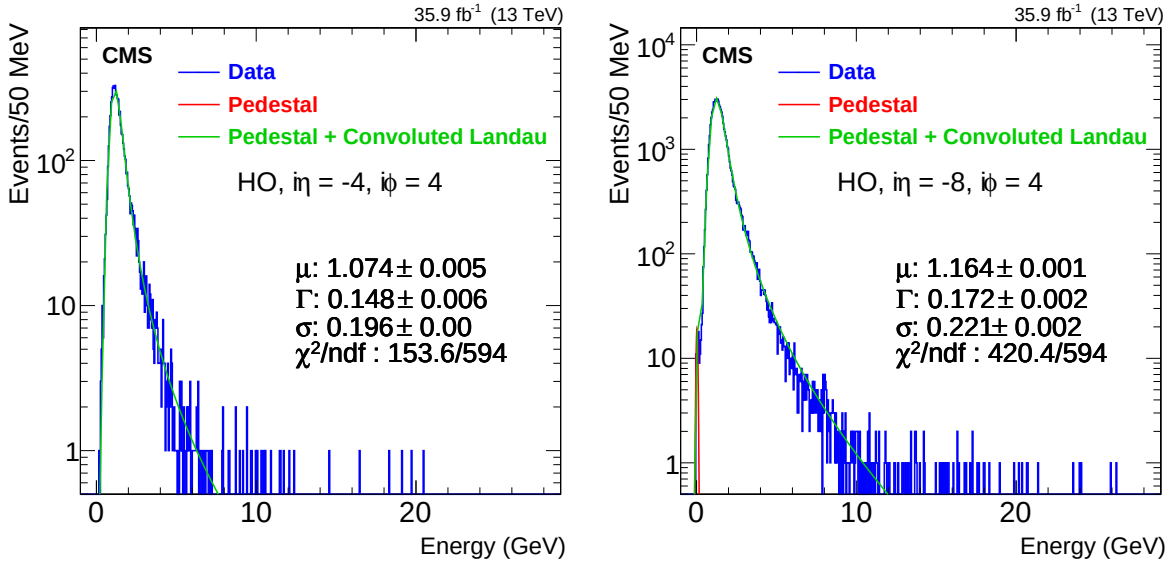

Figure 13: Energy distributions for HO towers impacted by a high-p_T muon for the central ring ($i\eta = -4$, $i\phi = 4$, left) and for a side ring ($i\eta = -8$, $i\phi = 4$, right), fitted with a combination of a Gaussian function for the pedestal region (shown as red lines) and a convolution of a Gaussian and a Landau function for the signal region (the combined fits are shown as the green lines). The parameters μ, Γ and σ are the most probable values and widths of the Landau and the Gaussian functions, and ndf is number of degrees of freedom in the fit.

a Gaussian function whose mean and width are set to values obtained from pedestal data, and with a convolution of Gaussian and Landau functions in the signal region, where width (σ) of the Gaussian function, the most probable value (μ), and width (Γ) of the Landau function are free parameters of the fit. The most probable values from the fits to the convoluted function are calculated for all towers. In parallel, the product of the path length of each muon trajectory in the tower and the ratio of the expected energy loss of the muon with respect to the energy loss at a fixed momentum (8 GeV) is calculated. These observed responses are then normalized over all ($i\eta$, $i\phi$) channels. These responses are then symmetrized over all $i\phi$ channels for a given $i\eta$ ring.

8.2 Absolute scale in the HO

In a test beam experiment [9], a 150 GeV muon beam was used to obtain the conversion factors from charge to energy for both the HB and HO. However, because the HO measures the energy deposited in the tail of a hadronic shower, which typically contains low-energy secondary particles, the energy resolution can be improved with the application of a weight factor to the HO energies. This weight factor was estimated using a test beam of 300 GeV π^- mesons [8].

The relative weight factor derived from a single particle test beam may not be optimal for jets, so the utility of an extra weight factor w_{HO} is explored. The value of w_{HO} is tested with collision data by balancing energies in dijet events, where one of the jets produces a substantial energy deposit in the HO. The analysis varies the scale of the HO energy deposits contributing to a PF jet to find the weight factor which gives the best jet energy resolution.

Events are selected with the following criteria:

- if there are more than two jets in the event, the third jet p_T is required to be less than 30 GeV,

- the two leading jets must have $\Delta\phi > \pi/2$, and
- the event must not contain any isolated photon, electron, or muon with $p_T > 20\,\text{GeV}$.

This analysis uses jets in $|\eta| < 0.34$ (which corresponds to the central HO ring) with the highest energy HO cluster. Figure 14 shows the width of the dijet energy balance distribution as a function of w_{HO}, where the energy balance (E_b) is defined as

$$E_b = 2\frac{(p_{T1} - p_{T2})}{(p_{T1} + p_{T2})}, \tag{14}$$

with p_{T1} and p_{T2} being the transverse momenta of the leading and the subleading jet, respectively. The smooth curves are results from fits to asymmetric parabolic function through the points, which is defined as,

$$\sigma(E_b) = p_0 + \alpha_{1,2}\,(w_{HO} - p_2)^2\,, \tag{15}$$

where $\alpha_{1,2}$ are used for $(w_{HO} - p_2) \geq 0$ and $(w_{HO} - p_2) < 0$, respectively, and p_0, α_1, α_2, and p_2 are parameters of the fit. Events containing jets with higher HO energy provide a better sensitivity to w_{HO}. The results imply that within the uncertainty of measurements the relative weight factor of HO in these events is the same as in the test beam. Similar analyses are carried out for the other HO rings (±1, ±2) as well.

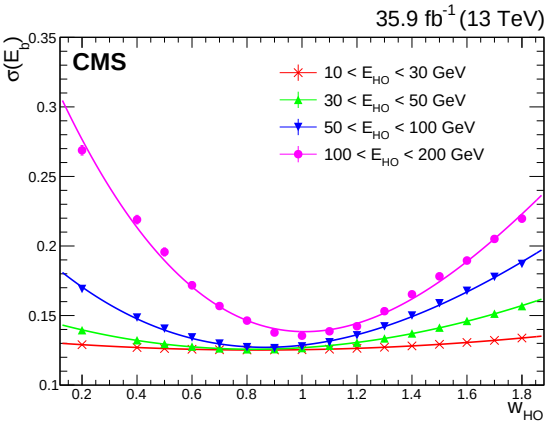

Figure 14: The Gaussian width of the relative difference of p_T of the two jets in dijet events as a function of HO weight factor in different ranges of energy contained in the HO cluster of the jet carrying the highest HO energy, when that jet is in ring 0. The smooth curves are results from fits to asymmetric parabolic function (Eq. (15)) through the points. Uncertainties are statistical only.

9 Summary

The CMS experiment utilizes a variety of data to calibrate the energy measurements obtained from its hadron calorimeter systems. The strategy utilizes different approaches since the calorimeter subdetectors make use of multiple technologies, have different radiation environments, and probe a large range of particle energies. The calibration is generally performed in two steps: the azimuthal (ϕ) intercalibration of the channels, followed by the determination of an absolute energy scale.

In the barrel, endcap, and forward calorimeters, the ϕ symmetry of minimum bias events is used to carry out an interdetector calibration, whereas the hadron outer calorimeter utilizes

reconstructed muons for this purpose. The absolute energy calibration of the barrel and endcap calorimeters is based on isolated charged hadrons with momenta between 40 and 60 GeV, whereas the calibration of the forward calorimeter relies on $Z \to ee$ events. The nonlinearity in the energy measurement of hadrons is addressed during the particle-flow reconstruction by using the predicted dependence on transverse momentum and pseudorapidity from a GEANT4-based simulation. Residual nonlinearities that affect the energy scale of reconstructed jets are reduced during the calibration of the jet energy scale. The calibration of the hadron outer calorimeter relies on the energy balance in dijet events.

The methods use proton-proton collision data at $\sqrt{s} = 13$ TeV collected with the CMS detector in 2016, and corresponding to integrated luminosities up to 35.9 fb^{-1}. The results are applied to the final reconstruction of events collected during that period. The systematic uncertainties in these measurements are dominated by systematic uncertainties in the amount of material between the interaction point and the detectors, including their dependence on azimuthal angle, and by the systematic uncertainties from the simulation of the effect of noise on the readout signal. These techniques lead to the final calibration precision of less than 3%.

Acknowledgments

We congratulate our colleagues in the CERN accelerator departments for the excellent performance of the LHC and thank the technical and administrative staffs at CERN and at other CMS institutes for their contributions to the success of the CMS effort. In addition, we gratefully acknowledge the computing centers and personnel of the Worldwide LHC Computing Grid for delivering so effectively the computing infrastructure essential to our analyses. Finally, we acknowledge the enduring support for the construction and operation of the LHC and the CMS detector provided by the following funding agencies: BMBWF and FWF (Austria); FNRS and FWO (Belgium); CNPq, CAPES, FAPERJ, FAPERGS, and FAPESP (Brazil); MES (Bulgaria); CERN; CAS, MoST, and NSFC (China); COLCIENCIAS (Colombia); MSES and CSF (Croatia); RPF (Cyprus); SENESCYT (Ecuador); MoER, ERC IUT, PUT and ERDF (Estonia); Academy of Finland, MEC, and HIP (Finland); CEA and CNRS/IN2P3 (France); BMBF, DFG, and HGF (Germany); GSRT (Greece); NKFIA (Hungary); DAE and DST (India); IPM (Iran); SFI (Ireland); INFN (Italy); MSIP and NRF (Republic of Korea); MES (Latvia); LAS (Lithuania); MOE and UM (Malaysia); BUAP, CINVESTAV, CONACYT, LNS, SEP, and UASLP-FAI (Mexico); MOS (Montenegro); MBIE (New Zealand); PAEC (Pakistan); MSHE and NSC (Poland); FCT (Portugal); JINR (Dubna); MON, RosAtom, RAS, RFBR, and NRC KI (Russia); MESTD (Serbia); SEIDI, CPAN, PCTI, and FEDER (Spain); MOSTR (Sri Lanka); Swiss Funding Agencies (Switzerland); MST (Taipei); ThEPCenter, IPST, STAR, and NSTDA (Thailand); TUBITAK and TAEK (Turkey); NASU (Ukraine); STFC (United Kingdom); DOE and NSF (USA).

Individuals have received support from the Marie-Curie program and the European Research Council and Horizon 2020 Grant, contract Nos. 675440, 752730, and 765710 (European Union); the Leventis Foundation; the A.P. Sloan Foundation; the Alexander von Humboldt Foundation; the Belgian Federal Science Policy Office; the Fonds pour la Formation à la Recherche dans l'Industrie et dans l'Agriculture (FRIA-Belgium); the Agentschap voor Innovatie door Wetenschap en Technologie (IWT-Belgium); the F.R.S.-FNRS and FWO (Belgium) under the "Excellence of Science – EOS" – be.h project n. 30820817; the Beijing Municipal Science & Technology Commission, No. Z181100004218003; the Ministry of Education, Youth and Sports (MEYS) of the Czech Republic; the Lendület ("Momentum") Program and the János Bolyai Research Scholarship of the Hungarian Academy of Sciences, the New National Excellence Program ÚNKP, the NKFIA research grants 123842, 123959, 124845, 124850, 125105, 128713, 128786,

and 129058 (Hungary); the Council of Science and Industrial Research, India; the HOMING PLUS program of the Foundation for Polish Science, cofinanced from European Union, Regional Development Fund, the Mobility Plus program of the Ministry of Science and Higher Education, the National Science Center (Poland), contracts Harmonia 2014/14/M/ST2/00428, Opus 2014/13/B/ST2/02543, 2014/15/B/ST2/03998, and 2015/19/B/ST2/02861, Sonata-bis 2012/07/E/ST2/01406; the National Priorities Research Program by Qatar National Research Fund; the Ministry of Science and Education, grant no. 3.2989.2017 (Russia); the Programa Estatal de Fomento de la Investigación Científica y Técnica de Excelencia María de Maeztu, grant MDM-2015-0509 and the Programa Severo Ochoa del Principado de Asturias; the Thalis and Aristeia programs cofinanced by EU-ESF and the Greek NSRF; the Rachadapisek Sompot Fund for Postdoctoral Fellowship, Chulalongkorn University and the Chulalongkorn Academic into Its 2nd Century Project Advancement Project (Thailand); the Nvidia Corporation; the Welch Foundation, contract C-1845; and the Weston Havens Foundation (USA).

References

[1] CMS Collaboration, "Measurement of the top quark mass using proton-proton data at $\sqrt{s}$ = 7 and 8 TeV", *Phys. Rev. D* **93** (2016) 072004, doi:10.1103/PhysRevD.93.072004, arXiv:1509.04044.

[2] CMS Collaboration, "Measurement of the top quark mass in the all-jets final state at $\sqrt{s}$ = 13 tev and combination with the lepton+jets channel", *Eur. Phys. J. C* **79** (2019) 313, doi:10.1140/epjc/s10052-019-6788-2, arXiv:1812.10534.

[3] ATLAS Collaboration, "Measurement of the W-boson mass in pp collisions at $\sqrt{s} = 7$ TeV with the ATLAS detector", *Eur. Phys. J. C* **78** (2018) 110, doi:10.1140/epjc/s10052-017-5475-4, arXiv:1701.07240.

[4] CMS Collaboration, "Search for dark matter, extra dimensions, and unparticles in monojet events in proton-proton collisions at $\sqrt{s}$ = 8 tev", *Eur. Phys. J. C* **75** (2015) 235, doi:10.1140/epjc/s10052-015-3451-4, arXiv:1408.3583.

[5] ATLAS Tile Calorimeter System Collaboration, "The laser calibration of the ATLAS tile calorimeter during the LHC run 1", *JINST* **11** (2016) T10005, doi:10.1088/1748-0221/11/10/T10005, arXiv:1608.02791.

[6] ATLAS Collaboration, "A measurement of the calorimeter response to single hadrons and determination of the jet energy scale uncertainty using LHC Run-1 pp-collision data with the ATLAS detector", *Eur. Phys. J. C* **77** (2017) 26, doi:10.1140/epjc/s10052-016-4580-0, arXiv:1607.08842.

[7] CMS HCAL Collaboration, "Studies of the response of the prototype CMS hadron calorimeter, including magnetic field effects, to pion, electron, and muon beams", *Nucl. Instrum. Meth. A* **457** (2001) 75, doi:10.1016/S0168-9002(00)00711-7, arXiv:hep-ex/0007045.

[8] CMS HCAL Collaboration, "Design, performance, and calibration of the CMS hadron-outer calorimeter", *Eur. Phys. J. C* **57** (2008) 653, doi:10.1140/epjc/s10052-008-0756-6.

[9] CMS HCAL/ECAL Collaboration, "The CMS barrel calorimeter response to particle beams from 2 to 350 GeV/c", *Eur. Phys. J. C* **60** (2009) 359, doi:10.1140/epjc/s10052-009-1024-0.

[10] ATLAS Liquid Argon EMEC/HEC Collaboration, "Hadronic calibration of the ATLAS liquid argon end-cap calorimeter in the pseudorapidity region $1.6 < |\eta| < 1.8$ in beam tests", *Nucl. Instrum. Meth. A* **531** (2004) 481, doi:10.1016/j.nima.2004.05.133, arXiv:physics/0407009.

[11] CMS Collaboration, "CMS hadron calorimeter technical design report", Technical Report CERN/LHCC 97-31, 1997.

[12] CMS Collaboration, "The CMS experiment at the CERN LHC", *JINST* **3** (2008) S08004, doi:10.1088/1748-0221/3/08/S08004.

[13] CMS HCAL Collaboration, "Design, performance, and calibration of CMS hadron-barrel calorimeter wedges", *Eur. Phys. J. C* **55** (2008) 159, doi:10.1140/epjc/s10052-008-0573-y.

[14] CMS HCAL Collaboration, "Design, performance and calibration of the CMS forward calorimeter wedges", *Eur. Phys. J. C* **53** (2008) 139, doi:10.1140/epjc/s10052-007-0459-4.

[15] E. Hazen et al., "Radioactive source calibration technique for the CMS hadron calorimeter", *Nucl. Instrum. Meth. A* **511** (2003) 311, doi:10.1016/S0168-9002(03)01971-5.

[16] CMS Collaboration, "Performance of the CMS hadron calorimeter with cosmic ray muons and LHC beam data", *JINST* **5** (2010) T03012, doi:10.1088/1748-0221/5/03/T03012, arXiv:0911.4991.

[17] CMS Collaboration, "Particle-flow reconstruction and global event description with the CMS detector", *JINST* **12** (2017) P10003, doi:10.1088/1748-0221/12/10/P10003, arXiv:1706.04965.

[18] GEANT4 Collaboration, "GEANT4–a simulation toolkit", *Nucl. Instrum. Meth. A* **506** (2003) 250, doi:10.1016/S0168-9002(03)01368-8.

[19] CMS Collaboration, "Jet energy scale and resolution in the CMS experiment in pp collisions at 8 TeV", *JINST* **12** (2017) P02014, doi:10.1088/1748-0221/12/02/P02014, arXiv:1607.03663.

[20] CMS Collaboration, "Performance of photon reconstruction and identification with the CMS detector in proton-proton collisions at $\sqrt{s} = 8$ TeV", *JINST* **10** (2015) P08010, doi:10.1088/1748-0221/10/08/P08010, arXiv:1502.02702.

[21] CMS Collaboration, "Description and performance of track and primary-vertex reconstruction with the CMS tracker", *JINST* **9** (2014) P10009, doi:10.1088/1748-0221/9/10/P10009, arXiv:1405.6569.

[22] CMS Collaboration, "The CMS trigger system", *JINST* **12** (2017) P01020, doi:10.1088/1748-0221/12/01/P01020, arXiv:1609.02366.

[23] P. Cushman, A. Heering, and A. Ronzhin, "Custom HPD readout for the CMS HCAL", *Nucl. Instrum. Meth. A* **442** (2000) 289, doi:10.1016/S0168-9002(99)01236-X.

[24] T. M. Shaw et al., "Front end readout electronics for the CMS hadron calorimeter", in *Nuclear Science Symposium Conference Record, 2002 IEEE*, p. 194. 2002. doi:10.1109/NSSMIC.2002.1239297.

[25] CMS HCAL Collaboration, "Dose rate effects in the radiation damage of the plastic scintillators of the CMS hadron endcap calorimeter", *JINST* **11** (2016) T10004, doi:10.1088/1748-0221/11/10/T10004, arXiv:1608.07267.

[26] R. A. Shukla et al., "Microscopic characterisation of photo detectors from CMS hadron calorimeter", *Rev. Sci. Instrum.* **90** (2019) 023303, doi:10.1063/1.5046465, arXiv:1806.09887.

[27] M. Cacciari, G. P. Salam, and G. Soyez, "The anti-k_{T} jet clustering algorithm", *JHEP* **04** (2008) 063, doi:10.1088/1126-6708/2008/04/063, arXiv:0802.1189.

[28] M. Cacciari, G. P. Salam, and G. Soyez, "FastJet user manual", *Eur. Phys. J. C* **72** (2012) 1896, doi:10.1140/epjc/s10052-012-1896-2, arXiv:1111.6097.

[29] T. Sjöstrand et al., "An introduction to Pythia 8.2", *Comput. Phys. Commun.* **191** (2015) 159, doi:10.1016/j.cpc.2015.01.024, arXiv:1410.3012.

[30] J. Alwall et al., "The automated computation of tree-level and next-to-leading order differential cross sections, and their matching to parton shower simulations", *JHEP* **07** (2014) 079, doi:10.1007/JHEP07(2014)079, arXiv:1405.0301.

[31] NNPDF Collaboration, "Parton distributions for the LHC Run II", *JHEP* **04** (2015) 040, doi:10.1007/JHEP04(2015)040, arXiv:1410.8849.

[32] CMS Collaboration, "Event generator tunes obtained from underlying event and multiparton scattering measurements", *Eur. Phys. J. C* **76** (2016) 155, doi:10.1140/epjc/s10052-016-3988-x, arXiv:1512.00815.

[33] CMS Collaboration, "Performance of electron reconstruction and selection with the CMS detector in proton-proton collisions at $\sqrt{s} = 8$ TeV", *JINST* **10** (2015) P06005, doi:10.1088/1748-0221/10/06/P06005, arXiv:1502.02701.

[34] Particle Data Group, "Review of particle physics", *Phys. Rev. D* **98** (2018) 030001, doi:10.1103/PhysRevD.98.030001.

[35] CMS Collaboration, "Performance of CMS muon reconstruction in pp collision events at $\sqrt{s} = 7$ TeV", *JINST* **7** (2012) P10002, doi:10.1088/1748-0221/7/10/P10002, arXiv:1206.4071.

A The CMS Collaboration

Yerevan Physics Institute, Yerevan, Armenia
A.M. Sirunyan[†], A. Tumasyan

Institut für Hochenergiephysik, Wien, Austria
W. Adam, F. Ambrogi, T. Bergauer, J. Brandstetter, M. Dragicevic, J. Erö, A. Escalante Del Valle, M. Flechl, R. Frühwirth[1], M. Jeitler[1], N. Krammer, I. Krätschmer, D. Liko, T. Madlener, I. Mikulec, N. Rad, J. Schieck[1], R. Schöfbeck, M. Spanring, D. Spitzbart, W. Waltenberger, C.-E. Wulz[1], M. Zarucki

Institute for Nuclear Problems, Minsk, Belarus
V. Chekhovsky, A. Litomin, V. Mossolov

Universiteit Antwerpen, Antwerpen, Belgium
M.R. Darwish, E.A. De Wolf, D. Di Croce, X. Janssen, A. Lelek, M. Pieters, H. Rejeb Sfar, H. Van Haevermaet, P. Van Mechelen, S. Van Putte, N. Van Remortel

Vrije Universiteit Brussel, Brussel, Belgium
F. Blekman, E.S. Bols, S.S. Chhibra, J. D'Hondt, J. De Clercq, D. Lontkovskyi, S. Lowette, I. Marchesini, S. Moortgat, L. Moreels, Q. Python, K. Skovpen, S. Tavernier, W. Van Doninck, P. Van Mulders, I. Van Parijs

Université Libre de Bruxelles, Bruxelles, Belgium
D. Beghin, B. Bilin, H. Brun, B. Clerbaux, G. De Lentdecker, H. Delannoy, B. Dorney, L. Favart, A. Grebenyuk, A.K. Kalsi, A. Popov, N. Postiau, E. Starling, L. Thomas, C. Vander Velde, P. Vanlaer, D. Vannerom

Ghent University, Ghent, Belgium
T. Cornelis, D. Dobur, I. Khvastunov[2], M. Niedziela, C. Roskas, D. Trocino, M. Tytgat, W. Verbeke, B. Vermassen, M. Vit, N. Zaganidis

Université Catholique de Louvain, Louvain-la-Neuve, Belgium
O. Bondu, G. Bruno, C. Caputo, P. David, C. Delaere, M. Delcourt, A. Giammanco, V. Lemaitre, A. Magitteri, J. Prisciandaro, A. Saggio, M. Vidal Marono, P. Vischia, J. Zobec

Centro Brasileiro de Pesquisas Fisicas, Rio de Janeiro, Brazil
F.L. Alves, G.A. Alves, G. Correia Silva, C. Hensel, A. Moraes, P. Rebello Teles

Universidade do Estado do Rio de Janeiro, Rio de Janeiro, Brazil
E. Belchior Batista Das Chagas, W. Carvalho, J. Chinellato[3], E. Coelho, E.M. Da Costa, G.G. Da Silveira[4], D. De Jesus Damiao, C. De Oliveira Martins, S. Fonseca De Souza, L.M. Huertas Guativa, H. Malbouisson, J. Martins[5], D. Matos Figueiredo, M. Medina Jaime[6], M. Melo De Almeida, C. Mora Herrera, L. Mundim, H. Nogima, W.L. Prado Da Silva, L.J. Sanchez Rosas, A. Santoro, A. Sznajder, M. Thiel, E.J. Tonelli Manganote[3], F. Torres Da Silva De Araujo, A. Vilela Pereira

Universidade Estadual Paulista [a], Universidade Federal do ABC [b], São Paulo, Brazil
C.A. Bernardes[a], L. Calligaris[a], T.R. Fernandez Perez Tomei[a], E.M. Gregores[b], D.S. Lemos, P.G. Mercadante[b], S.F. Novaes[a], SandraS. Padula[a]

Institute for Nuclear Research and Nuclear Energy, Bulgarian Academy of Sciences, Sofia, Bulgaria
A. Aleksandrov, G. Antchev, R. Hadjiiska, P. Iaydjiev, A. Marinov, M. Misheva, M. Rodozov, M. Shopova, G. Sultanov

University of Sofia, Sofia, Bulgaria
M. Bonchev, A. Dimitrov, T. Ivanov, L. Litov, B. Pavlov, P. Petkov

Beihang University, Beijing, China
W. Fang[7], X. Gao[7], L. Yuan

Institute of High Energy Physics, Beijing, China
M. Ahmad, G.M. Chen, H.S. Chen, M. Chen, C.H. Jiang, D. Leggat, H. Liao, Z. Liu, S.M. Shaheen[8], A. Spiezia, J. Tao, E. Yazgan, H. Zhang, S. Zhang[8], J. Zhao

State Key Laboratory of Nuclear Physics and Technology, Peking University, Beijing, China
A. Agapitos, Y. Ban, G. Chen, A. Levin, J. Li, L. Li, Q. Li, Y. Mao, S.J. Qian, D. Wang, Q. Wang

Tsinghua University, Beijing, China
Z. Hu, Y. Wang

Universidad de Los Andes, Bogota, Colombia
C. Avila, A. Cabrera, L.F. Chaparro Sierra, C. Florez, C.F. González Hernández, M.A. Segura Delgado

Universidad de Antioquia, Medellin, Colombia
J. Mejia Guisao, J.D. Ruiz Alvarez, C.A. Salazar González, N. Vanegas Arbelaez

University of Split, Faculty of Electrical Engineering, Mechanical Engineering and Naval Architecture, Split, Croatia
D. Giljanović, N. Godinovic, D. Lelas, I. Puljak, T. Sculac

University of Split, Faculty of Science, Split, Croatia
Z. Antunovic, M. Kovac

Institute Rudjer Boskovic, Zagreb, Croatia
V. Brigljevic, S. Ceci, D. Ferencek, K. Kadija, B. Mesic, M. Roguljic, A. Starodumov[9], T. Susa

University of Cyprus, Nicosia, Cyprus
M.W. Ather, A. Attikis, E. Erodotou, A. Ioannou, M. Kolosova, S. Konstantinou, G. Mavromanolakis, J. Mousa, C. Nicolaou, F. Ptochos, P.A. Razis, H. Rykaczewski, D. Tsiakkouri

Charles University, Prague, Czech Republic
M. Finger[10], M. Finger Jr.[10], A. Kveton, J. Tomsa

Escuela Politecnica Nacional, Quito, Ecuador
E. Ayala

Universidad San Francisco de Quito, Quito, Ecuador
E. Carrera Jarrin

Academy of Scientific Research and Technology of the Arab Republic of Egypt, Egyptian Network of High Energy Physics, Cairo, Egypt
Y. Assran[11,12], S. Elgammal[12]

National Institute of Chemical Physics and Biophysics, Tallinn, Estonia
S. Bhowmik, A. Carvalho Antunes De Oliveira, R.K. Dewanjee, K. Ehataht, M. Kadastik, M. Raidal, C. Veelken

Department of Physics, University of Helsinki, Helsinki, Finland
P. Eerola, L. Forthomme, H. Kirschenmann, K. Osterberg, M. Voutilainen

Helsinki Institute of Physics, Helsinki, Finland
F. Garcia, J. Havukainen, J.K. Heikkilä, T. Järvinen, V. Karimäki, M.S. Kim, R. Kinnunen, T. Lampén, K. Lassila-Perini, S. Laurila, S. Lehti, T. Lindén, P. Luukka, T. Mäenpää, H. Siikonen, E. Tuominen, J. Tuominiemi

Lappeenranta University of Technology, Lappeenranta, Finland
T. Tuuva

IRFU, CEA, Université Paris-Saclay, Gif-sur-Yvette, France
M. Besancon, F. Couderc, M. Dejardin, D. Denegri, B. Fabbro, J.L. Faure, F. Ferri, S. Ganjour, A. Givernaud, P. Gras, G. Hamel de Monchenault, P. Jarry, C. Leloup, E. Locci, J. Malcles, J. Rander, A. Rosowsky, M.Ö. Sahin, A. Savoy-Navarro[13], M. Titov

Laboratoire Leprince-Ringuet, Ecole polytechnique, CNRS/IN2P3, Université Paris-Saclay, Palaiseau, France
S. Ahuja, C. Amendola, F. Beaudette, P. Busson, C. Charlot, B. Diab, G. Falmagne, R. Granier de Cassagnac, I. Kucher, A. Lobanov, C. Martin Perez, M. Nguyen, C. Ochando, P. Paganini, J. Rembser, R. Salerno, J.B. Sauvan, Y. Sirois, A. Zabi, A. Zghiche

Université de Strasbourg, CNRS, IPHC UMR 7178, Strasbourg, France
J.-L. Agram[14], J. Andrea, D. Bloch, G. Bourgatte, J.-M. Brom, E.C. Chabert, C. Collard, E. Conte[14], J.-C. Fontaine[14], D. Gelé, U. Goerlach, M. Jansová, A.-C. Le Bihan, N. Tonon, P. Van Hove

Centre de Calcul de l'Institut National de Physique Nucleaire et de Physique des Particules, CNRS/IN2P3, Villeurbanne, France
S. Gadrat

Université de Lyon, Université Claude Bernard Lyon 1, CNRS-IN2P3, Institut de Physique Nucléaire de Lyon, Villeurbanne, France
S. Beauceron, C. Bernet, G. Boudoul, C. Camen, N. Chanon, R. Chierici, D. Contardo, P. Depasse, H. El Mamouni, J. Fay, S. Gascon, M. Gouzevitch, B. Ille, Sa. Jain, F. Lagarde, I.B. Laktineh, H. Lattaud, A. Lesauvage, M. Lethuillier, L. Mirabito, S. Perries, V. Sordini, L. Torterotot, G. Touquet, M. Vander Donckt, S. Viret

Georgian Technical University, Tbilisi, Georgia
G. Adamov

Tbilisi State University, Tbilisi, Georgia
Z. Tsamalaidze[10]

RWTH Aachen University, I. Physikalisches Institut, Aachen, Germany
C. Autermann, L. Feld, M.K. Kiesel, K. Klein, M. Lipinski, D. Meuser, A. Pauls, M. Preuten, M.P. Rauch, C. Schomakers, J. Schulz, M. Teroerde, B. Wittmer

RWTH Aachen University, III. Physikalisches Institut A, Aachen, Germany
A. Albert, M. Erdmann, S. Erdweg, T. Esch, B. Fischer, R. Fischer, S. Ghosh, T. Hebbeker, K. Hoepfner, H. Keller, L. Mastrolorenzo, M. Merschmeyer, A. Meyer, P. Millet, G. Mocellin, S. Mondal, S. Mukherjee, D. Noll, A. Novak, T. Pook, A. Pozdnyakov, T. Quast, M. Radziej, Y. Rath, H. Reithler, M. Rieger, J. Roemer, A. Schmidt, S.C. Schuler, A. Sharma, S. Thüer, S. Wiedenbeck, S. Zaleski

RWTH Aachen University, III. Physikalisches Institut B, Aachen, Germany
G. Flügge, W. Haj Ahmad[15], O. Hlushchenko, T. Kress, T. Müller, A. Nehrkorn, A. Nowack, C. Pistone, O. Pooth, D. Roy, H. Sert, A. Stahl[16]

Deutsches Elektronen-Synchrotron, Hamburg, Germany
M. Aldaya Martin, P. Asmuss, I. Babounikau, H. Bakhshiansohi, K. Beernaert, O. Behnke, U. Behrens, A. Bermúdez Martínez, D. Bertsche, A.A. Bin Anuar, K. Borras[17], V. Botta, A. Campbell, A. Cardini, P. Connor, S. Consuegra Rodríguez, C. Contreras-Campana, V. Danilov, A. De Wit, M.M. Defranchis, C. Diez Pardos, D. Domínguez Damiani, G. Eckerlin, D. Eckstein, T. Eichhorn, A. Elwood, E. Eren, E. Gallo[18], A. Geiser, J.M. Grados Luyando, A. Grohsjean, M. Guthoff, M. Haranko, A. Harb, A. Jafari, N.Z. Jomhari, H. Jung, A. Kasem[17], M. Kasemann, H. Kaveh, J. Keaveney, C. Kleinwort, J. Knolle, D. Krücker, W. Lange, T. Lenz, J. Leonard, J. Lidrych, K. Lipka, W. Lohmann[19], R. Mankel, I.-A. Melzer-Pellmann, A.B. Meyer, M. Meyer, M. Missiroli, G. Mittag, J. Mnich, A. Mussgiller, V. Myronenko, D. Pérez Adán, S.K. Pflitsch, D. Pitzl, A. Raspereza, A. Saibel, M. Savitskyi, V. Scheurer, P. Schütze, C. Schwanenberger, R. Shevchenko, A. Singh, H. Tholen, O. Turkot, A. Vagnerini, M. Van De Klundert, G.P. Van Onsem, R. Walsh, Y. Wen, K. Wichmann, C. Wissing, O. Zenaiev, R. Zlebcik

University of Hamburg, Hamburg, Germany
R. Aggleton, S. Bein, L. Benato, A. Benecke, V. Blobel, T. Dreyer, A. Ebrahimi, A. Fröhlich, C. Garbers, E. Garutti, D. Gonzalez, P. Gunnellini, J. Haller, A. Hinzmann, A. Karavdina, G. Kasieczka, R. Klanner, R. Kogler, N. Kovalchuk, S. Kurz, V. Kutzner, J. Lange, T. Lange, A. Malara, J. Multhaup, C.E.N. Niemeyer, A. Perieanu, A. Reimers, O. Rieger, C. Scharf, P. Schleper, S. Schumann, J. Schwandt, J. Sonneveld, H. Stadie, G. Steinbrück, F.M. Stober, M. Stöver, B. Vormwald, I. Zoi

Karlsruher Institut fuer Technologie, Karlsruhe, Germany
M. Akbiyik, C. Barth, M. Baselga, S. Baur, T. Berger, E. Butz, R. Caspart, T. Chwalek, W. De Boer, A. Dierlamm, K. El Morabit, N. Faltermann, M. Giffels, P. Goldenzweig, A. Gottmann, M.A. Harrendorf, F. Hartmann[16], U. Husemann, S. Kudella, S. Mitra, M.U. Mozer, D. Müller, Th. Müller, M. Musich, A. Nürnberg, G. Quast, K. Rabbertz, M. Schröder, I. Shvetsov, H.J. Simonis, R. Ulrich, M. Wassmer, M. Weber, C. Wöhrmann, R. Wolf

Institute of Nuclear and Particle Physics (INPP), NCSR Demokritos, Aghia Paraskevi, Greece
G. Anagnostou, P. Asenov, G. Daskalakis, T. Geralis, A. Kyriakis, D. Loukas, G. Paspalaki

National and Kapodistrian University of Athens, Athens, Greece
M. Diamantopoulou, G. Karathanasis, P. Kontaxakis, A. Manousakis-katsikakis, A. Panagiotou, I. Papavergou, N. Saoulidou, A. Stakia, K. Theofilatos, K. Vellidis, E. Vourliotis

National Technical University of Athens, Athens, Greece
G. Bakas, K. Kousouris, I. Papakrivopoulos, G. Tsipolitis

University of Ioánnina, Ioánnina, Greece
I. Evangelou, C. Foudas, P. Gianneios, P. Katsoulis, P. Kokkas, S. Mallios, K. Manitara, N. Manthos, I. Papadopoulos, J. Strologas, F.A. Triantis, D. Tsitsonis

MTA-ELTE Lendület CMS Particle and Nuclear Physics Group, Eötvös Loránd University, Budapest, Hungary
M. Bartók[20], R. Chudasama, M. Csanad, P. Major, K. Mandal, A. Mehta, M.I. Nagy, G. Pasztor, O. Surányi, G.I. Veres

Wigner Research Centre for Physics, Budapest, Hungary
G. Bencze, C. Hajdu, D. Horvath[21], F. Sikler, T.. Vámi, V. Veszpremi, G. Vesztergombi†

Institute of Nuclear Research ATOMKI, Debrecen, Hungary
N. Beni, S. Czellar, J. Karancsi[20], A. Makovec, J. Molnar, Z. Szillasi

Institute of Physics, University of Debrecen, Debrecen, Hungary
P. Raics, D. Teyssier, Z.L. Trocsanyi, B. Ujvari

Eszterhazy Karoly University, Karoly Robert Campus, Gyongyos, Hungary
T. Csorgo, W.J. Metzger, F. Nemes, T. Novak

Indian Institute of Science (IISc), Bangalore, India
S. Choudhury, J.R. Komaragiri, P.C. Tiwari

National Institute of Science Education and Research, HBNI, Bhubaneswar, India
S. Bahinipati[23], C. Kar, G. Kole, P. Mal, V.K. Muraleedharan Nair Bindhu, A. Nayak[24], D.K. Sahoo[23], S.K. Swain

Panjab University, Chandigarh, India
S. Bansal, S.B. Beri, V. Bhatnagar, S. Chauhan, R. Chawla, N. Dhingra, R. Gupta, A. Kaur, M. Kaur, S. Kaur, P. Kumari, M. Lohan, M. Meena, K. Sandeep, S. Sharma, J.B. Singh, A.K. Virdi, G. Walia

University of Delhi, Delhi, India
A. Bhardwaj, B.C. Choudhary, R.B. Garg, M. Gola, S. Keshri, Ashok Kumar, S. Malhotra, M. Naimuddin, P. Priyanka, K. Ranjan, Aashaq Shah, R. Sharma

Saha Institute of Nuclear Physics, HBNI, Kolkata, India
R. Bhardwaj[25], M. Bharti[25], R. Bhattacharya, S. Bhattacharya, U. Bhawandeep[25], D. Bhowmik, S. Dey, S. Dutta, S. Ghosh, M. Maity[26], K. Mondal, S. Nandan, A. Purohit, P.K. Rout, G. Saha, S. Sarkar, T. Sarkar[26], M. Sharan, B. Singh[25], S. Thakur[25]

Indian Institute of Technology Madras, Madras, India
P.K. Behera, P. Kalbhor, A. Muhammad, P.R. Pujahari, A. Sharma, A.K. Sikdar

Bhabha Atomic Research Centre, Mumbai, India
D. Dutta, V. Jha, V. Kumar, D.K. Mishra, P.K. Netrakanti, L.M. Pant, P. Shukla

Tata Institute of Fundamental Research-A, Mumbai, India
T. Aziz, M.A. Bhat, S. Dugad, G.B. Mohanty, P. Shingade, N. Sur, RavindraKumar Verma

Tata Institute of Fundamental Research-B, Mumbai, India
S. Banerjee, S. Bhattacharya, S. Chatterjee, P. Das, M. Guchait, S. Karmakar, M.M. Kolwalkar, S. Kumar, G. Majumder, K. Mazumdar, P. Patel, P. Pathare, M.R. Patil, N. Sahoo, S. Sawant

Indian Institute of Science Education and Research (IISER), Pune, India
S. Chauhan, S. Dube, V. Hegde, B. Kansal, A. Kapoor, K. Kothekar, S. Pandey, A. Rane, A. Rastogi, S. Sharma

Institute for Research in Fundamental Sciences (IPM), Tehran, Iran
S. Chenarani[27], E. Eskandari Tadavani, S.M. Etesami[27], M. Khakzad, M. Mohammadi Najafabadi, M. Naseri, F. Rezaei Hosseinabadi

University College Dublin, Dublin, Ireland
M. Felcini, M. Grunewald

INFN Sezione di Bari [a], Università di Bari [b], Politecnico di Bari [c], Bari, Italy
M. Abbrescia[a,b], R. Aly[a,b,28], C. Calabria[a,b], A. Colaleo[a], D. Creanza[a,c], L. Cristella[a,b], N. De Filippis[a,c], M. De Palma[a,b], A. Di Florio[a,b], L. Fiore[a], A. Gelmi[a,b], G. Iaselli[a,c],

M. Ince[a,b], S. Lezki[a,b], G. Maggi[a,c], M. Maggi[a], G. Miniello[a,b], S. My[a,b], S. Nuzzo[a,b], A. Pompili[a,b], G. Pugliese[a,c], R. Radogna[a], A. Ranieri[a], G. Selvaggi[a,b], L. Silvestris[a], R. Venditti[a], P. Verwilligen[a]

INFN Sezione di Bologna [a], Università di Bologna [b], Bologna, Italy
G. Abbiendi[a], C. Battilana[a,b], D. Bonacorsi[a,b], L. Borgonovi[a,b], S. Braibant-Giacomelli[a,b], R. Campanini[a,b], P. Capiluppi[a,b], A. Castro[a,b], F.R. Cavallo[a], C. Ciocca[a], G. Codispoti[a,b], M. Cuffiani[a,b], G.M. Dallavalle[a], F. Fabbri[a], A. Fanfani[a,b], E. Fontanesi[a,b], P. Giacomelli[a], C. Grandi[a], L. Guiducci[a,b], F. Iemmi[a,b], S. Lo Meo[a,29], S. Marcellini[a], G. Masetti[a], F.L. Navarria[a,b], A. Perrotta[a], F. Primavera[a,b], A.M. Rossi[a,b], T. Rovelli[a,b], G.P. Siroli[a,b], N. Tosi[a]

INFN Sezione di Catania [a], Università di Catania [b], Catania, Italy
S. Albergo[a,b,30], S. Costa[a,b], A. Di Mattia[a], R. Potenza[a,b], A. Tricomi[a,b,30], C. Tuve[a,b]

INFN Sezione di Firenze [a], Università di Firenze [b], Firenze, Italy
G. Barbagli[a], A. Cassese, R. Ceccarelli, K. Chatterjee[a,b], V. Ciulli[a,b], C. Civinini[a], R. D'Alessandro[a,b], E. Focardi[a,b], G. Latino[a,b], P. Lenzi[a,b], M. Meschini[a], S. Paoletti[a], G. Sguazzoni[a], D. Strom[a], L. Viliani[a]

INFN Laboratori Nazionali di Frascati, Frascati, Italy
L. Benussi, S. Bianco, D. Piccolo

INFN Sezione di Genova [a], Università di Genova [b], Genova, Italy
M. Bozzo[a,b], F. Ferro[a], R. Mulargia[a,b], E. Robutti[a], S. Tosi[a,b]

INFN Sezione di Milano-Bicocca [a], Università di Milano-Bicocca [b], Milano, Italy
A. Benaglia[a], A. Beschi[a,b], F. Brivio[a,b], V. Ciriolo[a,b,16], S. Di Guida[a,b,16], M.E. Dinardo[a,b], P. Dini[a], S. Gennai[a], A. Ghezzi[a,b], P. Govoni[a,b], L. Guzzi[a,b], M. Malberti[a], S. Malvezzi[a], D. Menasce[a], F. Monti[a,b], L. Moroni[a], G. Ortona[a,b], M. Paganoni[a,b], D. Pedrini[a], S. Ragazzi[a,b], T. Tabarelli de Fatis[a,b], D. Zuolo[a,b]

INFN Sezione di Napoli [a], Università di Napoli 'Federico II' [b], Napoli, Italy, Università della Basilicata [c], Potenza, Italy, Università G. Marconi [d], Roma, Italy
S. Buontempo[a], N. Cavallo[a,c], A. De Iorio[a,b], A. Di Crescenzo[a,b], F. Fabozzi[a,c], F. Fienga[a], G. Galati[a], A.O.M. Iorio[a,b], L. Lista[a,b], S. Meola[a,d,16], P. Paolucci[a,16], B. Rossi[a], C. Sciacca[a,b], E. Voevodina[a,b]

INFN Sezione di Padova [a], Università di Padova [b], Padova, Italy, Università di Trento [c], Trento, Italy
P. Azzi[a], N. Bacchetta[a], D. Bisello[a,b], A. Boletti[a,b], A. Bragagnolo[a,b], R. Carlin[a,b], P. Checchia[a], P. De Castro Manzano[a], T. Dorigo[a], U. Dosselli[a], F. Gasparini[a,b], U. Gasparini[a,b], A. Gozzelino[a], S.Y. Hoh[a,b], P. Lujan[a], M. Margoni[a,b], A.T. Meneguzzo[a,b], J. Pazzini[a,b], M. Presilla[b], P. Ronchese[a,b], R. Rossin[a,b], F. Simonetto[a,b], A. Tiko[a], M. Tosi[a,b], M. Zanetti[a,b], P. Zotto[a,b], G. Zumerle[a,b]

INFN Sezione di Pavia [a], Università di Pavia [b], Pavia, Italy
A. Braghieri[a], P. Montagna[a,b], S.P. Ratti[a,b], V. Re[a], M. Ressegotti[a,b], C. Riccardi[a,b], P. Salvini[a], I. Vai[a,b], P. Vitulo[a,b]

INFN Sezione di Perugia [a], Università di Perugia [b], Perugia, Italy
M. Biasini[a,b], G.M. Bilei[a], D. Ciangottini[a,b], L. Fanò[a,b], P. Lariccia[a,b], R. Leonardi[a,b], G. Mantovani[a,b], V. Mariani[a,b], M. Menichelli[a], A. Rossi[a,b], A. Santocchia[a,b], D. Spiga[a]

INFN Sezione di Pisa [a], Università di Pisa [b], Scuola Normale Superiore di Pisa [c], Pisa, Italy
K. Androsov[a], P. Azzurri[a], G. Bagliesi[a], V. Bertacchi[a,c], L. Bianchini[a], T. Boccali[a],

R. Castaldi[a], M.A. Ciocci[a,b], R. Dell'Orso[a], G. Fedi[a], L. Giannini[a,c], A. Giassi[a], M.T. Grippo[a], F. Ligabue[a,c], E. Manca[a,c], G. Mandorli[a,c], A. Messineo[a,b], F. Palla[a], A. Rizzi[a,b], G. Rolandi[31], S. Roy Chowdhury, A. Scribano[a], P. Spagnolo[a], R. Tenchini[a], G. Tonelli[a,b], N. Turini, A. Venturi[a], P.G. Verdini[a]

INFN Sezione di Roma [a], Sapienza Università di Roma [b], Rome, Italy
F. Cavallari[a], M. Cipriani[a,b], D. Del Re[a,b], E. Di Marco[a,b], M. Diemoz[a], E. Longo[a,b], B. Marzocchi[a,b], P. Meridiani[a], G. Organtini[a,b], F. Pandolfi[a], R. Paramatti[a,b], C. Quaranta[a,b], S. Rahatlou[a,b], C. Rovelli[a], F. Santanastasio[a,b], L. Soffi[a,b]

INFN Sezione di Torino [a], Università di Torino [b], Torino, Italy, Università del Piemonte Orientale [c], Novara, Italy
N. Amapane[a,b], R. Arcidiacono[a,c], S. Argiro[a,b], M. Arneodo[a,c], N. Bartosik[a], R. Bellan[a,b], C. Biino[a], A. Cappati[a,b], N. Cartiglia[a], S. Cometti[a], M. Costa[a,b], R. Covarelli[a,b], N. Demaria[a], B. Kiani[a,b], C. Mariotti[a], S. Maselli[a], E. Migliore[a,b], V. Monaco[a,b], E. Monteil[a,b], M. Monteno[a], M.M. Obertino[a,b], L. Pacher[a,b], N. Pastrone[a], M. Pelliccioni[a], G.L. Pinna Angioni[a,b], A. Romero[a,b], M. Ruspa[a,c], R. Sacchi[a,b], R. Salvatico[a,b], V. Sola[a], A. Solano[a,b], D. Soldi[a,b], A. Staiano[a]

INFN Sezione di Trieste [a], Università di Trieste [b], Trieste, Italy
S. Belforte[a], V. Candelise[a,b], M. Casarsa[a], F. Cossutti[a], A. Da Rold[a,b], G. Della Ricca[a,b], F. Vazzoler[a,b], A. Zanetti[a]

Kyungpook National University, Daegu, Korea
B. Kim, D.H. Kim, G.N. Kim, J. Lee, S.W. Lee, C.S. Moon, Y.D. Oh, S.I. Pak, S. Sekmen, D.C. Son, Y.C. Yang

Chonnam National University, Institute for Universe and Elementary Particles, Kwangju, Korea
H. Kim, D.H. Moon, G. Oh

Hanyang University, Seoul, Korea
B. Francois, T.J. Kim, J. Park

Korea University, Seoul, Korea
S. Cho, S. Choi, Y. Go, D. Gyun, S. Ha, B. Hong, K. Lee, K.S. Lee, J. Lim, J. Park, S.K. Park, Y. Roh, J. Yoo

Kyung Hee University, Department of Physics
J. Goh

Sejong University, Seoul, Korea
H.S. Kim

Seoul National University, Seoul, Korea
J. Almond, J.H. Bhyun, J. Choi, S. Jeon, J. Kim, J.S. Kim, H. Lee, K. Lee, S. Lee, K. Nam, M. Oh, S.B. Oh, B.C. Radburn-Smith, U.K. Yang, H.D. Yoo, I. Yoon, G.B. Yu

University of Seoul, Seoul, Korea
D. Jeon, H. Kim, J.H. Kim, J.S.H. Lee, I.C. Park, I. Watson

Sungkyunkwan University, Suwon, Korea
Y. Choi, C. Hwang, Y. Jeong, J. Lee, Y. Lee, I. Yu

Riga Technical University, Riga, Latvia
V. Veckalns[32]

Vilnius University, Vilnius, Lithuania
V. Dudenas, A. Juodagalvis, G. Tamulaitis, J. Vaitkus

National Centre for Particle Physics, Universiti Malaya, Kuala Lumpur, Malaysia
Z.A. Ibrahim, F. Mohamad Idris[33], W.A.T. Wan Abdullah, M.N. Yusli, Z. Zolkapli

Universidad de Sonora (UNISON), Hermosillo, Mexico
J.F. Benitez, A. Castaneda Hernandez, J.A. Murillo Quijada, L. Valencia Palomo

Centro de Investigacion y de Estudios Avanzados del IPN, Mexico City, Mexico
H. Castilla-Valdez, E. De La Cruz-Burelo, I. Heredia-De La Cruz[34], R. Lopez-Fernandez, A. Sanchez-Hernandez

Universidad Iberoamericana, Mexico City, Mexico
S. Carrillo Moreno, C. Oropeza Barrera, M. Ramirez-Garcia, F. Vazquez Valencia

Benemerita Universidad Autonoma de Puebla, Puebla, Mexico
J. Eysermans, I. Pedraza, H.A. Salazar Ibarguen, C. Uribe Estrada

Universidad Autónoma de San Luis Potosí, San Luis Potosí, Mexico
A. Morelos Pineda

University of Montenegro, Podgorica, Montenegro
N. Raicevic

University of Auckland, Auckland, New Zealand
D. Krofcheck

University of Canterbury, Christchurch, New Zealand
S. Bheesette, P.H. Butler

National Centre for Physics, Quaid-I-Azam University, Islamabad, Pakistan
A. Ahmad, M. Ahmad, Q. Hassan, H.R. Hoorani, W.A. Khan, M.A. Shah, M. Shoaib, M. Waqas

AGH University of Science and Technology Faculty of Computer Science, Electronics and Telecommunications, Krakow, Poland
V. Avati, L. Grzanka, M. Malawski

National Centre for Nuclear Research, Swierk, Poland
H. Bialkowska, M. Bluj, B. Boimska, M. Górski, M. Kazana, M. Szleper, P. Zalewski

Institute of Experimental Physics, Faculty of Physics, University of Warsaw, Warsaw, Poland
K. Bunkowski, A. Byszuk[35], K. Doroba, A. Kalinowski, M. Konecki, J. Krolikowski, M. Misiura, M. Olszewski, A. Pyskir, M. Walczak

Laboratório de Instrumentação e Física Experimental de Partículas, Lisboa, Portugal
M. Araujo, P. Bargassa, D. Bastos, A. Di Francesco, P. Faccioli, B. Galinhas, M. Gallinaro, J. Hollar, N. Leonardo, J. Seixas, K. Shchelina, G. Strong, O. Toldaiev, J. Varela

Joint Institute for Nuclear Research, Dubna, Russia
S. Afanasiev, P. Bunin, M. Gavrilenko, I. Golutvin, I. Gorbunov, A. Kamenev, V. Karjavine, A. Lanev, A. Malakhov, V. Matveev[36,37], P. Moisenz, V. Palichik, V. Perelygin, M. Savina, S. Shmatov, S. Shulha, N. Skatchkov, V. Smirnov, N. Voytishin, A. Zarubin

Petersburg Nuclear Physics Institute, Gatchina (St. Petersburg), Russia
L. Chtchipounov, V. Golovtcov, Y. Ivanov, V. Kim[38], E. Kuznetsova[39], P. Levchenko, V. Murzin, V. Oreshkin, I. Smirnov, D. Sosnov, V. Sulimov, L. Uvarov, A. Vorobyev

Institute for Nuclear Research, Moscow, Russia
Yu. Andreev, A. Dermenev, S. Gninenko, N. Golubev, A. Karneyeu, M. Kirsanov, N. Krasnikov, A. Pashenkov, D. Tlisov, A. Toropin

Institute for Theoretical and Experimental Physics named by A.I. Alikhanov of NRC 'Kurchatov Institute', Moscow, Russia
V. Epshteyn, V. Gavrilov, N. Lychkovskaya, A. Nikitenko[40], V. Popov, I. Pozdnyakov, G. Safronov, A. Spiridonov, A. Stepennov, M. Toms, E. Vlasov, A. Zhokin

Moscow Institute of Physics and Technology, Moscow, Russia
T. Aushev

National Research Nuclear University 'Moscow Engineering Physics Institute' (MEPhI), Moscow, Russia
M. Chadeeva[41], P. Parygin, D. Philippov, E. Popova, V. Rusinov

P.N. Lebedev Physical Institute, Moscow, Russia
V. Andreev, M. Azarkin, I. Dremin, M. Kirakosyan, A. Terkulov

Skobeltsyn Institute of Nuclear Physics, Lomonosov Moscow State University, Moscow, Russia
A. Belyaev, E. Boos, A. Demiyanov, L. Dudko, A. Ershov, A. Gribushin, A. Kaminskiy[42], V. Klyukhin, O. Kodolova, I. Lokhtin, S. Obraztsov, S. Petrushanko, V. Savrin

Novosibirsk State University (NSU), Novosibirsk, Russia
A. Barnyakov[43], V. Blinov[43], T. Dimova[43], L. Kardapoltsev[43], Y. Skovpen[43]

Institute for High Energy Physics of National Research Centre 'Kurchatov Institute', Protvino, Russia
I. Azhgirey, I. Bayshev, S. Bitioukov, V. Kachanov, D. Konstantinov, P. Mandrik, V. Petrov, R. Ryutin, S. Slabospitskii, A. Sobol, S. Troshin, N. Tyurin, A. Uzunian, A. Volkov

National Research Tomsk Polytechnic University, Tomsk, Russia
A. Babaev, A. Iuzhakov, V. Okhotnikov

Tomsk State University, Tomsk, Russia
V. Borchsh, V. Ivanchenko, E. Tcherniaev

University of Belgrade: Faculty of Physics and VINCA Institute of Nuclear Sciences
P. Adzic[44], P. Cirkovic, D. Devetak, M. Dordevic, P. Milenovic, J. Milosevic, M. Stojanovic

Centro de Investigaciones Energéticas Medioambientales y Tecnológicas (CIEMAT), Madrid, Spain
M. Aguilar-Benitez, J. Alcaraz Maestre, A. lvarez Fernández, I. Bachiller, M. Barrio Luna, J.A. Brochero Cifuentes, C.A. Carrillo Montoya, M. Cepeda, M. Cerrada, N. Colino, B. De La Cruz, A. Delgado Peris, C. Fernandez Bedoya, J.P. Fernández Ramos, J. Flix, M.C. Fouz, O. Gonzalez Lopez, S. Goy Lopez, J.M. Hernandez, M.I. Josa, D. Moran, . Navarro Tobar, A. Pérez-Calero Yzquierdo, J. Puerta Pelayo, I. Redondo, L. Romero, S. Sánchez Navas, M.S. Soares, A. Triossi, C. Willmott

Universidad Autónoma de Madrid, Madrid, Spain
C. Albajar, J.F. de Trocóniz

Universidad de Oviedo, Instituto Universitario de Ciencias y Tecnologías Espaciales de Asturias (ICTEA), Oviedo, Spain
B. Alvarez Gonzalez, J. Cuevas, C. Erice, J. Fernandez Menendez, S. Folgueras, I. Gonzalez Caballero, J.R. González Fernández, E. Palencia Cortezon, V. Rodríguez Bouza, S. Sanchez Cruz

Instituto de Física de Cantabria (IFCA), CSIC-Universidad de Cantabria, Santander, Spain
I.J. Cabrillo, A. Calderon, B. Chazin Quero, J. Duarte Campderros, M. Fernandez, P.J. Fernández Manteca, A. García Alonso, G. Gomez, C. Martinez Rivero, P. Martinez Ruiz del Arbol, F. Matorras, J. Piedra Gomez, C. Prieels, T. Rodrigo, A. Ruiz-Jimeno, L. Russo[45], L. Scodellaro, N. Trevisani, I. Vila, J.M. Vizan Garcia

University of Colombo, Colombo, Sri Lanka
K. Malagalage

University of Ruhuna, Department of Physics, Matara, Sri Lanka
W.G.D. Dharmaratna, N. Wickramage

CERN, European Organization for Nuclear Research, Geneva, Switzerland
D. Abbaneo, B. Akgun, E. Auffray, G. Auzinger, J. Baechler, P. Baillon, A.H. Ball, D. Barney, J. Bendavid, M. Bianco, A. Bocci, P. Bortignon, E. Bossini, C. Botta, E. Brondolin, T. Camporesi, A. Caratelli, G. Cerminara, E. Chapon, G. Cucciati, D. d'Enterria, A. Dabrowski, N. Daci, V. Daponte, A. David, O. Davignon, A. De Roeck, N. Deelen, M. Deile, M. Dobson, M. Dünser, N. Dupont, A. Elliott-Peisert, F. Fallavollita[46], D. Fasanella, S. Fiorendi, G. Franzoni, J. Fulcher, W. Funk, S. Giani, D. Gigi, A. Gilbert, K. Gill, F. Glege, M. Gruchala, M. Guilbaud, D. Gulhan, J. Hegeman, C. Heidegger, Y. Iiyama, V. Innocente, P. Janot, O. Karacheban[19], J. Kaspar, J. Kieseler, M. Krammer[1], C. Lange, P. Lecoq, C. Lourenço, L. Malgeri, M. Mannelli, A. Massironi, F. Meijers, J.A. Merlin, S. Mersi, E. Meschi, F. Moortgat, M. Mulders, J. Ngadiuba, S. Nourbakhsh, S. Orfanelli, L. Orsini, F. Pantaleo[16], L. Pape, E. Perez, M. Peruzzi, A. Petrilli, G. Petrucciani, A. Pfeiffer, M. Pierini, F.M. Pitters, D. Rabady, A. Racz, M. Rovere, H. Sakulin, C. Schäfer, C. Schwick, M. Selvaggi, A. Sharma, P. Silva, W. Snoeys, P. Sphicas[47], J. Steggemann, S. Summers, V.R. Tavolaro, D. Treille, A. Tsirou, A. Vartak, M. Verzetti, W.D. Zeuner

Paul Scherrer Institut, Villigen, Switzerland
L. Caminada[48], K. Deiters, W. Erdmann, R. Horisberger, Q. Ingram, H.C. Kaestli, D. Kotlinski, U. Langenegger, T. Rohe, S.A. Wiederkehr

ETH Zurich - Institute for Particle Physics and Astrophysics (IPA), Zurich, Switzerland
M. Backhaus, P. Berger, N. Chernyavskaya, G. Dissertori, M. Dittmar, M. Donegà, C. Dorfer, T.A. Gómez Espinosa, C. Grab, D. Hits, T. Klijnsma, W. Lustermann, R.A. Manzoni, M. Marionneau, M.T. Meinhard, F. Micheli, P. Musella, F. Nessi-Tedaldi, F. Pauss, G. Perrin, L. Perrozzi, S. Pigazzini, M.G. Ratti, M. Reichmann, C. Reissel, T. Reitenspiess, D. Ruini, D.A. Sanz Becerra, M. Schönenberger, L. Shchutska, M.L. Vesterbacka Olsson, R. Wallny, D.H. Zhu

Universität Zürich, Zurich, Switzerland
T.K. Aarrestad, C. Amsler[49], D. Brzhechko, M.F. Canelli, A. De Cosa, R. Del Burgo, S. Donato, B. Kilminster, S. Leontsinis, V.M. Mikuni, I. Neutelings, G. Rauco, P. Robmann, D. Salerno, K. Schweiger, C. Seitz, Y. Takahashi, S. Wertz, A. Zucchetta

National Central University, Chung-Li, Taiwan
T.H. Doan, C.M. Kuo, W. Lin, A. Roy, S.S. Yu

National Taiwan University (NTU), Taipei, Taiwan

P. Chang, Y. Chao, K.F. Chen, P.H. Chen, W.-S. Hou, Y.y. Li, R.-S. Lu, E. Paganis, A. Psallidas, A. Steen

Chulalongkorn University, Faculty of Science, Department of Physics, Bangkok, Thailand
B. Asavapibhop, C. Asawatangtrakuldee, N. Srimanobhas, N. Suwonjandee

ukurova University, Physics Department, Science and Art Faculty, Adana, Turkey
D. Agyel, S. Anagul, M.N. Bakirci[50], A. Bat, F. Bilican, F. Boran, A. Celik[51], S. Cerci[52], S. Damarseckin[53], Z.S. Demiroglu, F. Dolek, C. Dozen, I. Dumanoglu, E. Eskut, G. Gokbulut, EmineGurpinar Guler[54], Y. Guler, I. Hos[55], C. Isik, E.E. Kangal[56], O. Kara, A. Kayis Topaksu, U. Kiminsu, M. Oglakci, G. Onengut, K. Ozdemir[57], S. Ozturk[50], A. Polatoz, A.E. Simsek, . Sözbilir, D. Sunar Cerci[52], B. Tali[52], U.G. Tok, H. Topakli[50], S. Turkcapar, E. Uslan, I.S. Zorbakir, C. Zorbilmez

Middle East Technical University, Physics Department, Ankara, Turkey
B. Isildak[58], G. Karapinar[59], M. Yalvac

Bogazici University, Istanbul, Turkey
I.O. Atakisi, E. Gülmez, M. Kaya[60], O. Kaya[61], B. Kaynak, Ö. Özçelik, S. Tekten, E.A. Yetkin[62]

Istanbul Technical University, Istanbul, Turkey
A. Cakir, K. Cankocak, Y. Komurcu, S. Sen[63]

Istanbul University, Istanbul, Turkey
S. Ozkorucuklu

Institute for Scintillation Materials of National Academy of Science of Ukraine, Kharkov, Ukraine
B. Grynyov

National Scientific Center, Kharkov Institute of Physics and Technology, Kharkov, Ukraine
L. Levchuk

University of Bristol, Bristol, United Kingdom
F. Ball, E. Bhal, S. Bologna, J.J. Brooke, D. Burns[64], E. Clement, D. Cussans, H. Flacher, J. Goldstein, G.P. Heath, H.F. Heath, L. Kreczko, S. Paramesvaran, B. Penning, T. Sakuma, S. Seif El Nasr-Storey, D. Smith[64], V.J. Smith, J. Taylor, A. Titterton

Rutherford Appleton Laboratory, Didcot, United Kingdom
K.W. Bell, A. Belyaev[65], C. Brew, R.M. Brown, D. Cieri, D.J.A. Cockerill, J.A. Coughlan, K. Harder, S. Harper, J. Linacre, K. Manolopoulos, D.M. Newbold, E. Olaiya, D. Petyt, T. Reis, T. Schuh, C.H. Shepherd-Themistocleous, A. Thea, I.R. Tomalin, T. Williams, W.J. Womersley

Imperial College, London, United Kingdom
R. Bainbridge, P. Bloch, J. Borg, S. Breeze, O. Buchmuller, A. Bundock, GurpreetSingh CHAHAL[66], D. Colling, P. Dauncey, G. Davies, M. Della Negra, R. Di Maria, P. Everaerts, G. Hall, G. Iles, T. James, M. Komm, C. Laner, L. Lyons, A.-M. Magnan, S. Malik, A. Martelli, V. Milosevic, J. Nash[67], V. Palladino, M. Pesaresi, D.M. Raymond, A. Richards, A. Rose, E. Scott, C. Seez, A. Shtipliyski, M. Stoye, T. Strebler, A. Tapper, K. Uchida, T. Virdee[16], N. Wardle, D. Winterbottom, J. Wright, A.G. Zecchinelli, S.C. Zenz

Brunel University, Uxbridge, United Kingdom
J.E. Cole, P.R. Hobson, A. Khan, P. Kyberd, C.K. Mackay, A. Morton, I.D. Reid, L. Teodorescu, S. Zahid

Baylor University, Waco, USA
K. Call, J. Dittmann, K. Hatakeyama, C. Madrid, B. McMaster, N. Pastika, C. Smith

Catholic University of America, Washington, DC, USA
R. Bartek, A. Dominguez, R. Uniyal

The University of Alabama, Tuscaloosa, USA
A. Buccilli, S.I. Cooper, C. Henderson, P. Rumerio, C. West

Boston University, Boston, USA
D. Arcaro, C. Cosby, Z. Demiragli, D. Gastler, S. Girgis, E. Hazen, D. Pinna, C. Richardson, J. Rohlf, D. Sperka, I. Suarez, L. Sulak, S. Wu, D. Zou

Brown University, Providence, USA
G. Benelli, B. Burkle, X. Coubez[17], D. Cutts, Y.t. Duh, M. Hadley, J. Hakala, U. Heintz, J.M. Hogan[68], K.H.M. Kwok, E. Laird, G. Landsberg, J. Lee, Z. Mao, M. Narain, S. Sagir[69], R. Syarif, E. Usai, D. Yu, W. Zhang

University of California, Davis, Davis, USA
R. Band, C. Brainerd, R. Breedon, M. Calderon De La Barca Sanchez, M. Chertok, J. Conway, R. Conway, P.T. Cox, R. Erbacher, C. Flores, G. Funk, F. Jensen, W. Ko, O. Kukral, R. Lander, M. Mulhearn, D. Pellett, J. Pilot, M. Shi, D. Taylor, K. Tos, M. Tripathi, Z. Wang, F. Zhang

University of California, Los Angeles, USA
M. Bachtis, C. Bravo, R. Cousins, A. Dasgupta, A. Florent, J. Hauser, M. Ignatenko, N. Mccoll, W.A. Nash, S. Regnard, D. Saltzberg, C. Schnaible, B. Stone, V. Valuev

University of California, Riverside, Riverside, USA
K. Burt, Y. Chen, R. Clare, J.W. Gary, S.M.A. Ghiasi Shirazi, G. Hanson, G. Karapostoli, E. Kennedy, O.R. Long, M. Olmedo Negrete, M.I. Paneva, W. Si, L. Wang, H. Wei, S. Wimpenny, B.R. Yates, Y. Zhang

University of California, San Diego, La Jolla, USA
J.G. Branson, P. Chang, S. Cittolin, M. Derdzinski, R. Gerosa, D. Gilbert, B. Hashemi, D. Klein, V. Krutelyov, J. Letts, M. Masciovecchio, S. May, S. Padhi, M. Pieri, V. Sharma, M. Tadel, F. Würthwein, A. Yagil, G. Zevi Della Porta

University of California, Santa Barbara - Department of Physics, Santa Barbara, USA
N. Amin, R. Bhandari, C. Campagnari, M. Citron, V. Dutta, M. Franco Sevilla, L. Gouskos, J. Incandela, B. Marsh, H. Mei, A. Ovcharova, H. Qu, J. Richman, U. Sarica, D. Stuart, S. Wang

California Institute of Technology, Pasadena, USA
D. Anderson, A. Bornheim, O. Cerri, I. Dutta, J.M. Lawhorn, N. Lu, J. Mao, H.B. Newman, T.Q. Nguyen, J. Pata, M. Spiropulu, J.R. Vlimant, S. Xie, Z. Zhang, R.Y. Zhu

Carnegie Mellon University, Pittsburgh, USA
M.B. Andrews, T. Ferguson, T. Mudholkar, M. Paulini, M. Sun, I. Vorobiev, M. Weinberg

University of Colorado Boulder, Boulder, USA
J.P. Cumalat, W.T. Ford, A. Johnson, E. MacDonald, T. Mulholland, R. Patel, A. Perloff, K. Stenson, K.A. Ulmer, S.R. Wagner

Cornell University, Ithaca, USA
J. Alexander, J. Chaves, Y. Cheng, J. Chu, A. Datta, A. Frankenthal, K. Mcdermott, J.R. Patterson, D. Quach, A. Rinkevicius[70], A. Ryd, S.M. Tan, Z. Tao, J. Thom, P. Wittich, M. Zientek

Fairfield University, Fairfield, USA
D. Winn

Fermi National Accelerator Laboratory, Batavia, USA
S. Abdullin, M. Albrow, M. Alyari, G. Apollinari, A. Apresyan, A. Apyan, S. Banerjee, L.A.T. Bauerdick, A. Beretvas, J. Berryhill, P.C. Bhat, K. Burkett, J.N. Butler, A. Canepa, G.B. Cerati, H.W.K. Cheung, F. Chlebana, M. Cremonesi, J. Duarte, V.D. Elvira, J. Freeman, Z. Gecse, E. Gottschalk, L. Gray, D. Green, S. Grünendahl, O. Gutsche, AllisonReinsvold Hall, J. Hanlon, R.M. Harris, S. Hasegawa, R. Heller, J. Hirschauer, B. Jayatilaka, S. Jindariani, M. Johnson, U. Joshi, B. Klima, M.J. Kortelainen, B. Kreis, S. Lammel, J. Lewis, D. Lincoln, R. Lipton, M. Liu, T. Liu, J. Lykken, K. Maeshima, J.M. Marraffino, D. Mason, P. McBride, P. Merkel, S. Mrenna, S. Nahn, V. O'Dell, V. Papadimitriou, K. Pedro, C. Pena, G. Rakness, F. Ravera, L. Ristori, B. Schneider, E. Sexton-Kennedy, N. Smith, A. Soha, W.J. Spalding, L. Spiegel, S. Stoynev, J. Strait, N. Strobbe, L. Taylor, S. Tkaczyk, N.V. Tran, L. Uplegger, E.W. Vaandering, C. Vernieri, M. Verzocchi, R. Vidal, M. Wang, H.A. Weber

University of Florida, Gainesville, USA
D. Acosta, P. Avery, D. Bourilkov, A. Brinkerhoff, L. Cadamuro, A. Carnes, V. Cherepanov, D. Curry, F. Errico, R.D. Field, S.V. Gleyzer, B.M. Joshi, M. Kim, J. Konigsberg, A. Korytov, K.H. Lo, P. Ma, K. Matchev, N. Menendez, G. Mitselmakher, D. Rosenzweig, K. Shi, J. Wang, S. Wang, X. Zuo

Florida International University, Miami, USA
Y.R. Joshi

Florida State University, Tallahassee, USA
T. Adams, A. Askew, S. Hagopian, V. Hagopian, K.F. Johnson, R. Khurana, T. Kolberg, G. Martinez, T. Perry, H. Prosper, C. Schiber, R. Yohay, J. Zhang

Florida Institute of Technology, Melbourne, USA
M.M. Baarmand, V. Bhopatkar, M. Hohlmann, D. Noonan, M. Rahmani, M. Saunders, F. Yumiceva

University of Illinois at Chicago (UIC), Chicago, USA
M.R. Adams, L. Apanasevich, D. Berry, R.R. Betts, R. Cavanaugh, X. Chen, S. Dittmer, O. Evdokimov, C.E. Gerber, D.A. Hangal, D.J. Hofman, K. Jung, C. Mills, T. Roy, M.B. Tonjes, N. Varelas, J. Viinikainen, H. Wang, X. Wang, Z. Wu

The University of Iowa, Iowa City, USA
M. Alhusseini, B. Bilki[54], W. Clarida, P. Debbins, K. Dilsiz[71], S. Durgut, L. Emediato, R.P. Gandrajula, M. Haytmyradov, V. Khristenko, O.K. Köseyan, T. Mcdowell, J.-P. Merlo, A. Mestvirishvili[72], M.J. Miller, A. Moeller, J. Nachtman, H. Ogul[73], Y. Onel, F. Ozok[74], A. Penzo, C. Rude, I. Schmidt, C. Snyder, D. Southwick, E. Tiras, J. Wetzel, K. Yi

Johns Hopkins University, Baltimore, USA
B. Blumenfeld, A. Cocoros, N. Eminizer, D. Fehling, L. Feng, A.V. Gritsan, W.T. Hung, P. Maksimovic, J. Roskes, M. Swartz, M. Xiao

The University of Kansas, Lawrence, USA
C. Baldenegro Barrera, P. Baringer, A. Bean, S. Boren, J. Bowen, A. Bylinkin, T. Isidori, S. Khalil, J. King, G. Krintiras, A. Kropivnitskaya, C. Lindsey, D. Majumder, W. Mcbrayer, N. Minafra, M. Murray, C. Rogan, C. Royon, S. Sanders, E. Schmitz, J.D. Tapia Takaki, Q. Wang, J. Williams, G. Wilson

Kansas State University, Manhattan, USA
S. Duric, A. Ivanov, K. Kaadze, D. Kim, Y. Maravin, D.R. Mendis, T. Mitchell, A. Modak, A. Mohammadi

Lawrence Livermore National Laboratory, Livermore, USA
F. Rebassoo, D. Wright

University of Maryland, College Park, USA
A. Baden, O. Baron, A. Belloni, S.C. Eno, Y. Feng, T. Grassi, N.J. Hadley, S. Jabeen, G.Y. Jeng, R.G. Kellogg, J. Kunkle, A.C. Mignerey, S. Nabili, F. Ricci-Tam, M. Seidel, Y.H. Shin, A. Skuja, S.C. Tonwar, K. Wong

Massachusetts Institute of Technology, Cambridge, USA
D. Abercrombie, B. Allen, A. Baty, R. Bi, S. Brandt, W. Busza, I.A. Cali, M. D'Alfonso, G. Gomez Ceballos, M. Goncharov, P. Harris, D. Hsu, M. Hu, M. Klute, D. Kovalskyi, Y.-J. Lee, P.D. Luckey, B. Maier, A.C. Marini, C. Mcginn, C. Mironov, S. Narayanan, X. Niu, C. Paus, D. Rankin, C. Roland, G. Roland, Z. Shi, G.S.F. Stephans, K. Sumorok, K. Tatar, D. Velicanu, J. Wang, T.W. Wang, B. Wyslouch

University of Minnesota, Minneapolis, USA
A.C. Benvenuti[†], R.M. Chatterjee, A. Evans, S. Guts, P. Hansen, J. Hiltbrand, Y. Kubota, Z. Lesko, J. Mans, R. Rusack, M.A. Wadud

University of Mississippi, Oxford, USA
J.G. Acosta, S. Oliveros

University of Nebraska-Lincoln, Lincoln, USA
K. Bloom, D.R. Claes, C. Fangmeier, L. Finco, F. Golf, R. Gonzalez Suarez, R. Kamalieddin, I. Kravchenko, J.E. Siado, G.R. Snow, B. Stieger, W. Tabb

State University of New York at Buffalo, Buffalo, USA
G. Agarwal, C. Harrington, I. Iashvili, A. Kharchilava, C. McLean, D. Nguyen, A. Parker, J. Pekkanen, S. Rappoccio, B. Roozbahani

Northeastern University, Boston, USA
G. Alverson, E. Barberis, C. Freer, Y. Haddad, A. Hortiangtham, G. Madigan, D.M. Morse, T. Orimoto, L. Skinnari, A. Tishelman-Charny, T. Wamorkar, B. Wang, A. Wisecarver, D. Wood

Northwestern University, Evanston, USA
S. Bhattacharya, J. Bueghly, T. Gunter, K.A. Hahn, N. Odell, M.H. Schmitt, K. Sung, M. Trovato, M. Velasco

University of Notre Dame, Notre Dame, USA
R. Bucci, N. Dev, R. Goldouzian, A.H. Heering, M. Hildreth, K. Hurtado Anampa, C. Jessop, D.J. Karmgard, K. Lannon, W. Li, N. Loukas, N. Marinelli, I. Mcalister, F. Meng, C. Mueller, Y. Musienko[36], M. Planer, R. Ruchti, P. Siddireddy, G. Smith, S. Taroni, M. Wayne, A. Wightman, M. Wolf, A. Woodard

The Ohio State University, Columbus, USA
J. Alimena, B. Bylsma, L.S. Durkin, S. Flowers, B. Francis, C. Hill, W. Ji, A. Lefeld, T.Y. Ling, B.L. Winer

Princeton University, Princeton, USA
S. Cooperstein, G. Dezoort, P. Elmer, J. Hardenbrook, N. Haubrich, S. Higginbotham,

A. Kalogeropoulos, S. Kwan, D. Lange, M.T. Lucchini, J. Luo, D. Marlow, K. Mei, I. Ojalvo, J. Olsen, C. Palmer, P. Piroué, J. Salfeld-Nebgen, D. Stickland, C. Tully, Z. Wang

University of Puerto Rico, Mayaguez, USA
S. Malik, S. Norberg

Purdue University, West Lafayette, USA
A. Barker, V.E. Barnes, S. Das, L. Gutay, M. Jones, A.W. Jung, A. Khatiwada, B. Mahakud, D.H. Miller, G. Negro, N. Neumeister, C.C. Peng, S. Piperov, H. Qiu, J.F. Schulte, J. Sun, F. Wang, R. Xiao, W. Xie

Purdue University Northwest, Hammond, USA
T. Cheng, J. Dolen, N. Parashar

Rice University, Houston, USA
K.M. Ecklund, S. Freed, F.J.M. Geurts, M. Kilpatrick, Arun Kumar, W. Li, B.P. Padley, R. Redjimi, J. Roberts, J. Rorie, W. Shi, A.G. Stahl Leiton, Z. Tu, A. Zhang

University of Rochester, Rochester, USA
A. Bodek, P. de Barbaro, R. Demina, J.L. Dulemba, C. Fallon, T. Ferbel, M. Galanti, A. Garcia-Bellido, J. Han, O. Hindrichs, A. Khukhunaishvili, E. Ranken, P. Tan, R. Taus

The Rockefeller University, New York, USA
R. Ciesielski

Rutgers, The State University of New Jersey, Piscataway, USA
B. Chiarito, J.P. Chou, A. Gandrakota, Y. Gershtein, E. Halkiadakis, A. Hart, M. Heindl, E. Hughes, S. Kaplan, S. Kyriacou, I. Laflotte, A. Lath, R. Montalvo, K. Nash, M. Osherson, H. Saka, S. Salur, S. Schnetzer, D. Sheffield, S. Somalwar, R. Stone, S. Thomas, P. Thomassen

University of Tennessee, Knoxville, USA
H. Acharya, A.G. Delannoy, G. Riley, S. Spanier

Texas A&M University, College Station, USA
O. Bouhali[75], M. Dalchenko, M. De Mattia, A. Delgado, S. Dildick, R. Eusebi, J. Gilmore, T. Huang, T. Kamon[76], S. Luo, D. Marley, R. Mueller, D. Overton, L. Perniè, D. Rathjens, A. Safonov

Texas Tech University, Lubbock, USA
N. Akchurin, J. Damgov, F. De Guio, S. Kunori, K. Lamichhane, S.W. Lee, T. Mengke, S. Muthumuni, T. Peltola, S. Undleeb, I. Volobouev, Z. Wang, A. Whitbeck

Vanderbilt University, Nashville, USA
S. Greene, A. Gurrola, R. Janjam, W. Johns, C. Maguire, A. Melo, H. Ni, K. Padeken, F. Romeo, P. Sheldon, S. Tuo, J. Velkovska, M. Verweij

University of Virginia, Charlottesville, USA
M.W. Arenton, P. Barria, B. Cox, G. Cummings, R. Hirosky, M. Joyce, A. Ledovskoy, C. Neu, B. Tannenwald, Y. Wang, E. Wolfe, F. Xia

Wayne State University, Detroit, USA
R. Harr, P.E. Karchin, N. Poudyal, J. Sturdy, P. Thapa

University of Wisconsin - Madison, Madison, WI, USA
T. Bose, J. Buchanan, C. Caillol, D. Carlsmith, S. Dasu, I. De Bruyn, L. Dodd, F. Fiori, C. Galloni, B. Gomber[77], H. He, M. Herndon, A. Hervé, U. Hussain, P. Klabbers, A. Lanaro, A. Loeliger,

K. Long, R. Loveless, J. Madhusudanan Sreekala, T. Ruggles, A. Savin, V. Sharma, W.H. Smith, D. Teague, S. Trembath-reichert, N. Woods

†: Deceased
1: Also at Vienna University of Technology, Vienna, Austria
2: Also at IRFU, CEA, Université Paris-Saclay, Gif-sur-Yvette, France
3: Also at Universidade Estadual de Campinas, Campinas, Brazil
4: Also at Federal University of Rio Grande do Sul, Porto Alegre, Brazil
5: Also at UFMS, Nova Andradina, Brazil
6: Also at Universidade Federal de Pelotas, Pelotas, Brazil
7: Also at Université Libre de Bruxelles, Bruxelles, Belgium
8: Also at University of Chinese Academy of Sciences, Beijing, China
9: Also at Institute for Theoretical and Experimental Physics named by A.I. Alikhanov of NRC 'Kurchatov Institute', Moscow, Russia
10: Also at Joint Institute for Nuclear Research, Dubna, Russia
11: Also at Suez University, Suez, Egypt
12: Now at British University in Egypt, Cairo, Egypt
13: Also at Purdue University, West Lafayette, USA
14: Also at Université de Haute Alsace, Mulhouse, France
15: Also at Erzincan Binali Yildirim University, Erzincan, Turkey
16: Also at CERN, European Organization for Nuclear Research, Geneva, Switzerland
17: Also at RWTH Aachen University, III. Physikalisches Institut A, Aachen, Germany
18: Also at University of Hamburg, Hamburg, Germany
19: Also at Brandenburg University of Technology, Cottbus, Germany
20: Also at Institute of Physics, University of Debrecen, Debrecen, Hungary, Debrecen, Hungary
21: Also at Institute of Nuclear Research ATOMKI, Debrecen, Hungary
22: Also at MTA-ELTE Lendület CMS Particle and Nuclear Physics Group, Eötvös Loránd University, Budapest, Hungary, Budapest, Hungary
23: Also at IIT Bhubaneswar, Bhubaneswar, India, Bhubaneswar, India
24: Also at Institute of Physics, Bhubaneswar, India
25: Also at Shoolini University, Solan, India
26: Also at University of Visva-Bharati, Santiniketan, India
27: Also at Isfahan University of Technology, Isfahan, Iran
28: Now at INFN Sezione di Bari [a], Università di Bari [b], Politecnico di Bari [c], Bari, Italy
29: Also at Italian National Agency for New Technologies, Energy and Sustainable Economic Development, Bologna, Italy
30: Also at Centro Siciliano di Fisica Nucleare e di Struttura Della Materia, Catania, Italy
31: Also at Scuola Normale e Sezione dell'INFN, Pisa, Italy
32: Also at Riga Technical University, Riga, Latvia, Riga, Latvia
33: Also at Malaysian Nuclear Agency, MOSTI, Kajang, Malaysia
34: Also at Consejo Nacional de Ciencia y Tecnología, Mexico City, Mexico
35: Also at Warsaw University of Technology, Institute of Electronic Systems, Warsaw, Poland
36: Also at Institute for Nuclear Research, Moscow, Russia
37: Now at National Research Nuclear University 'Moscow Engineering Physics Institute' (MEPhI), Moscow, Russia
38: Also at St. Petersburg State Polytechnical University, St. Petersburg, Russia
39: Also at University of Florida, Gainesville, USA
40: Also at Imperial College, London, United Kingdom
41: Also at P.N. Lebedev Physical Institute, Moscow, Russia

42: Also at INFN Sezione di Padova [a], Università di Padova [b], Padova, Italy, Università di Trento [c], Trento, Italy, Padova, Italy
43: Also at Budker Institute of Nuclear Physics, Novosibirsk, Russia
44: Also at Faculty of Physics, University of Belgrade, Belgrade, Serbia
45: Also at Università degli Studi di Siena, Siena, Italy
46: Also at INFN Sezione di Pavia [a], Università di Pavia [b], Pavia, Italy, Pavia, Italy
47: Also at National and Kapodistrian University of Athens, Athens, Greece
48: Also at Universität Zürich, Zurich, Switzerland
49: Also at Stefan Meyer Institute for Subatomic Physics, Vienna, Austria, Vienna, Austria
50: Also at Gaziosmanpasa University, Tokat, Turkey
51: Also at Burdur Mehmet Akif Ersoy University, BURDUR, Turkey
52: Also at Adiyaman University, Adiyaman, Turkey
53: Also at Şırnak University, Sirnak, Turkey
54: Also at Beykent University, Istanbul, Turkey, Istanbul, Turkey
55: Also at Istanbul Aydin University, Istanbul, Turkey
56: Also at Mersin University, Mersin, Turkey
57: Also at Piri Reis University, Istanbul, Turkey
58: Also at Ozyegin University, Istanbul, Turkey
59: Also at Izmir Institute of Technology, Izmir, Turkey
60: Also at Marmara University, Istanbul, Turkey
61: Also at Kafkas University, Kars, Turkey
62: Also at Istanbul Bilgi University, Istanbul, Turkey
63: Also at Hacettepe University, Ankara, Turkey
64: Also at Vrije Universiteit Brussel, Brussel, Belgium
65: Also at School of Physics and Astronomy, University of Southampton, Southampton, United Kingdom
66: Also at IPPP Durham University, Durham, United Kingdom
67: Also at Monash University, Faculty of Science, Clayton, Australia
68: Also at Bethel University, St. Paul, Minneapolis, USA, St. Paul, USA
69: Also at Karamanoğlu Mehmetbey University, Karaman, Turkey
70: Also at Vilnius University, Vilnius, Lithuania
71: Also at Bingol University, Bingol, Turkey
72: Also at Georgian Technical University, Tbilisi, Georgia
73: Also at Sinop University, Sinop, Turkey
74: Also at Mimar Sinan University, Istanbul, Istanbul, Turkey
75: Also at Texas A&M University at Qatar, Doha, Qatar
76: Also at Kyungpook National University, Daegu, Korea, Daegu, Korea
77: Also at University of Hyderabad, Hyderabad, India